MDPI

Article

Geochemical Characteristics and Metallogenic Significance of the X03 Vein Tourmaline in the Jiajika Rare Metal Deposit, West Sichuan

Yan Qin [1], Yang Li [1,2], Chenghui Wang [1,*], Lijun Liu [3,*], Kejun Hou [1] and Qian Wang [1]

1   Intitute of Mineral Resources, Chinese Academy of Geological Sciences, Beijing 100037, China;
    happyqinyan@sina.com (Y.Q.); liyangcdut@163.com (Y.L.); kejunhou@126.com (K.H.);
    doublefish17@163.com (Q.W.)
2   School of Earth Science, Chengdu University of Technology, Chengdu 610059, China
3   Sichuan Geological and Mineral Resources (Group) Co., Ltd., Chengdu 610031, China
*   Correspondence: wangchenghui@mail.cgs.gov.cn (C.W.); liulijunmails@163.com (L.L.)

Abstract: The Jiajika rare metal deposit contains the largest area of granitic pegmatite-type rare metal deposits in China. The X03 vein is an immense rare metal deposit dominated by lithium, which was found in the deposit in recent years. The contact metamorphic belt of tourmalinization and petrochemistry is widely developed in its wall rocks, and the altered rocks formed contain Li and other rare metal mineralization. In this paper, the tourmaline found in the different rocks of the Jiajika X03 vein is divided into four types: two-mica quartz schist (Tur-I), tourmaline hornfels (Tur-II), tourmaline-bearing granite pegmatite (Tur-III) and spodumene-bearing granite pegmatite (Tur-IV); their in situ major element, trace element and boron isotope data are systematically studied. The results show that all tourmalines in the Jiajika X03 vein deposit belong to the alkali group, and are schorl–Oxy/Fluor–schorl, dravite–Hydroxy-dravite and foitite–Oxy foitite solid solutions, among which Tur-I are dravite, Tur-II are foitite of hydrothermal origin and Tur-III and Tur-IV are schorl of magmatic origin. The boron isotope values show that the boron involved the formation process of tourmaline mainly originates from the Majingzi S-type granite, and the boron isotope variations in tourmaline are controlled by melt fluid and Rayleigh fractionation. Moreover, there is a clear correlation between the B isotope value of tourmaline and the Li, Mn, Zn, Mg, and V contents, showing that these contents in tourmaline are good indicators of the mineralization type of pegmatite.

Keywords: Jiajika X03 vein; tourmaline genesis; boron isotope; metallogenic indication

1. Introduction

Tourmaline is a boron silicate mineral with a complex chemical composition and crystal structure, is widely distributed in granite and granitic pegmatite, and is a main carrier of boron in acidic melts [1]. B has two isotopes, ^{10}B and ^{11}B, in nature. Due to the large mass difference between the two isotopes, isotopic fractionation is more significant in geological processes [2,3]. Trumbull et al. [4] systematically determined the B isotope and Li contents of tourmaline in rare metal pegmatite from Borborema Province, Brazil, and showed that the contents of Li, F, Mn, and Al in tourmaline from the edge to the core of the pegmatite deposit increased while the $\delta^{11}B$ value decreased. The lithium tourmaline inside the middle band also showed a decreasing trend in the $\delta^{11}B$ value from the core to the edge. Siegel et al. [5] studied the Varutrask pegmatite in northern Sweden and found that the $\delta^{11}B$ values of tourmaline showed regular changes from nonmineralized pegmatite zonation to lithium-rich pegmatite zonation. The crystallization of tourmaline and muscovite in pegmatite and the distribution of B isotopes between melt and fluid were the main reasons for the variation in tourmaline $\delta^{11}B$ values. Feng et al. [6] found that the trace element content and B isotope composition of schorl could effectively indicate the mineralization type of pegmatite

through a comprehensive analysis of the geochemical characteristics of tourmaline in granite-pegmatite in the East Qinling Mountains. Therefore, it is necessary to explore the chemical composition and boron isotope characteristics of tourmaline microregions in order to understand the magmatic-hydrothermal evolution of granite and granite-pegmatite and the properties and sources of ore-forming fluids [4,5,7–13].

The Jiajika deposit is the largest pegmatitic lithium polymetallic deposit in China [14]. Tourmaline is a widely distributed accessory mineral in the Jiajika deposit and is located in the orebody, surrounding rock and contact zone. Tourmaline contains almost all rock-forming elements and important volatile components, such as B, F and OH, which are often closely related to mineralization. Therefore, these are often used as the prospecting indications of W-Sn deposits and rare metal deposits [15]. At present, the mineralogical and geochemical characteristics of different types of tourmaline in the Jiajika deposit are very limited. Further study is needed to determine whether the variation in tourmaline composition can reflect the degree of differentiation between the Jiajika pegmatite and the surrounding rock contact zone and indicate the type of mineralization. In this paper, a systematic study on the petrography, major and trace elements and B isotopes of tourmaline in the contact zone between the pegmatite and surrounding rock of the Jiajika X03 vein was carried out to obtain the properties and evolutionary process of the ore-forming fluid through the variation in the tourmaline series components along with the evolution of pegmatite and to explore the indicative role of the tourmaline components and boron isotopes on mineralization.

2. Regional Geological Characteristics

The huge Songpan–Ganzi-Tianshuihai orogenic belt spans more than 2800 km in the eastern Tibetan Plateau and is famous for its immense lithium deposits, such as those in Jiajika and Kerin in western Sichuan and Bailongshan in Xinjiang [16]. Since the late Mesozoic, the orogenic belt has undergone multilevel napped-slip, accompanied by partial crustal melting; the flysch in the Triassic Xikang Group has undergone nonaxial bidirectional compression and contraction in the north–south and east–west directions and contains many synorogenic granites and postorogenic granites from 228 to 195 Ma [14]. The granite magmatic diapir or disassembled dome was formed in the cross-superposition area of the dorsal structure [17,18]. These magmatic diapiric domes are mainly composed of core continental crust remelting S-type granitic claves or hidden granite bases, peripheral granite-pegmatite and Barro-type and Bakken-type metamorphic rocks. These granites are all S-type peraluminous to strongly peraluminous granites [19]. Thousands of granite-pegmatite (ore) veins are present around these granites, and the rare metal mineral resources associated with them are very rich. Lithium, beryllium, niobium, tantalum, rubidium (cesium) and other minerals have been found in more than 70 places in western Sichuan. Based on the production characteristics of cluster belts, they can be divided into the Shiqu-Zhaoolong rare metal forming area, Kangding-Yajiang rare metal forming area (Jiajika deposit), Maerkangchuan rare metal forming area (Kerin field) and Jiulong rare metal forming area (Figure 1). These deposits together constitute the largest granite pegmatite type rare metal ore field in China [20–25].
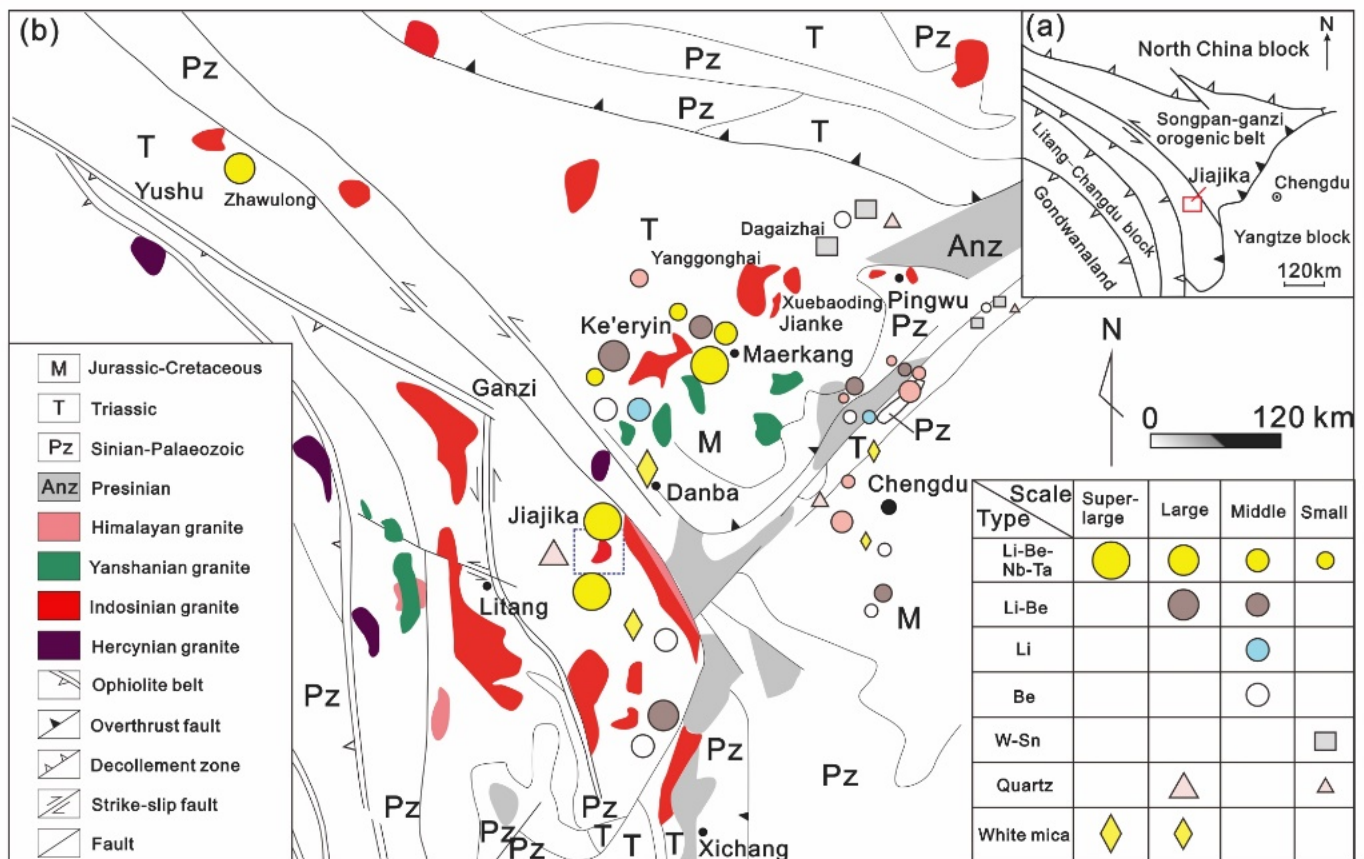
Figure 1. (**a**) Regional structure map of western Sichuan; (**b**) Distribution map of rare metal deposits in western Sichuan (modified from [18]).

2.1. Geological Characteristics of the Jiajika Deposit

In Kangding City, Ganzi Prefecture, Sichuan Province, on the eastern margin of the Qinghai-Tibet Plateau, the Jiajika pegmatite-type rare metal deposit is part of the Bayanjara-Songpan metallogenic province in the northeastern Tethys metallogenic domain (Figure 1) and the northern Bayanjara-Malkan Au–Ni–Pge–Fe–Mn–Pb–Li–Be-muscovite metallogenic belt. The Jinchuan-Danba Li–Be–Pb–Zn–Au-white mica metallogenic subbelt [25] is the largest area of rich solid lithium deposits in China. The deposits are characterized by a large-scale, a rich grade and multiple ore species, forming a complete Li-Be-Nb-Ta metallogenic series [23,24].

The Jiajika deposit is in the Yajiang structure-magmatic dome-shaped metamorphic group in the middle part of the Yajiang passive continental margin of the central fold and nappe belt in the central part of the Songpan-Ganzi orogenic belt [25,26]. The Jiajika deposit is controlled by a tectonic-magmatic dome, which is composed of granites, pegmatite dikes, and tectonic-thermal tectonic schist formed by the Zhuwo Formation, Xinduqiao Formation and sandy flysch in the Lower Triassic Xikang Group (Figure 2). To the south of the deposit, there is a 5.3 km^2 of the Indochina granite pluton, which is called the Majingzi pluton. The main lithology of the Majingzi pluton is medium- to fine-grained two-mica granite, with 10~50 m banded fine-grained two-mica granite at the top and side and a residual roof composed of cordierite and tourmaline hornfels at the top (indicating shallow denudation of the pluton). The two-mica granite of the Majingzi pluton is a high-potassium calc-alkaline peraluminous S-type granite enriched in rare metal metallogenic elements, such as Li, Be, Cs, Rb, Ta, Hf, W, and Sn, and complex agent elements, such as F, but it is poor in Zr, Sr and Ba. The highest values of Li and F are 443×10^{-6} and 2900×10^{-6}, respectively, indicating that the granite is a Li-F granite that is rich in rare metals and has good metallogenic conditions. Pegmatite dikes developed in groups in the top of the

Majingzi pluton and the periphery of the dome in the Jiajika deposit and show successive zonation outward from the center of the granitic pluton: microcline type (I) → microcline albite type (II) → albite type (III) → spodumene type (IV) → lepidolite (muscovite) (V) → quartz vein [14,27,28]. Spatially, the rare ore-forming elements are zoned from the center outward, and this zonation is roughly Be → Li → Nb + Ta → Cs. This zonal distribution provides only a general picture of the distribution of pegmatite in the deposit. Different types of dikes can also overlap or mix into zones.
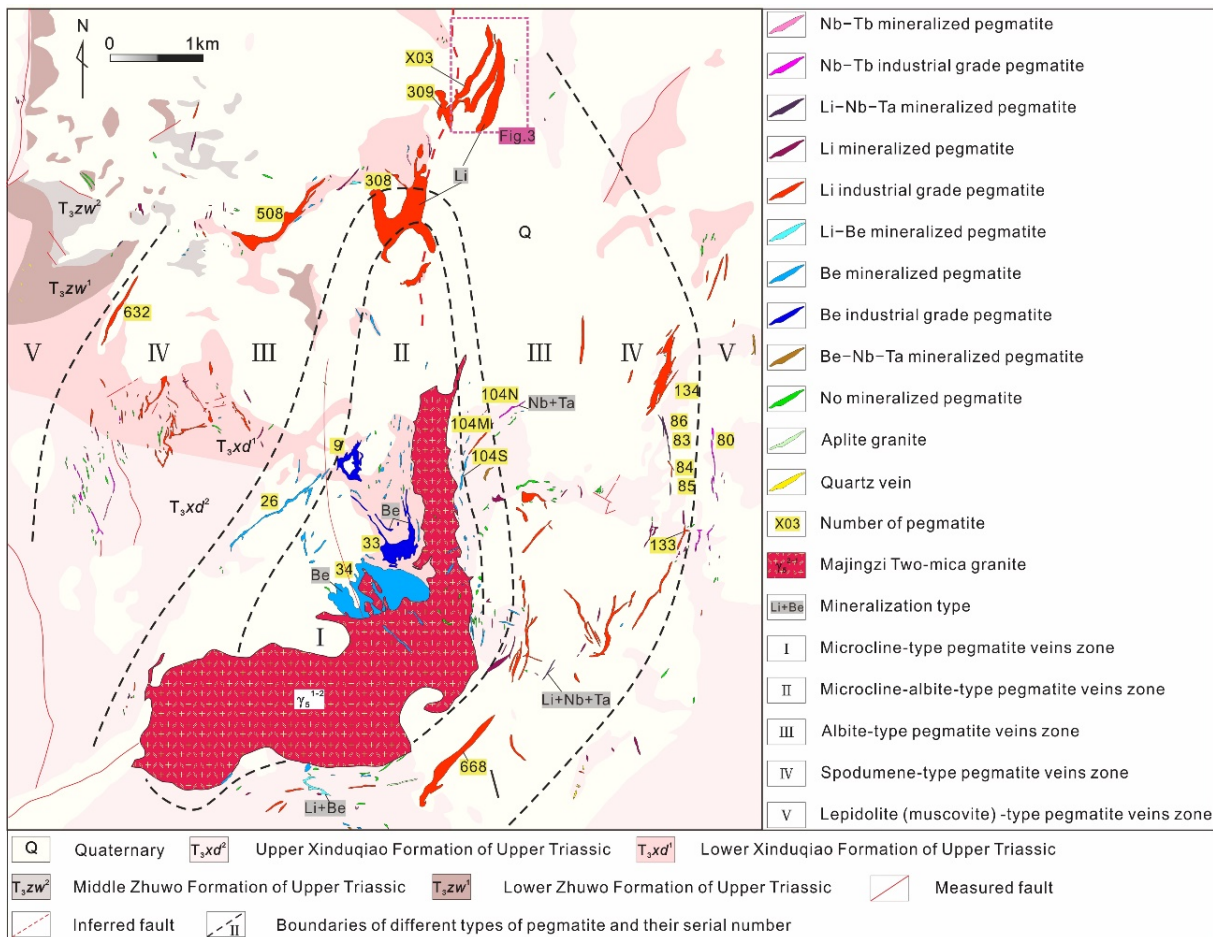

Figure 2. Geological map of the Jiajika deposit (Modified from [20]).

2.2. Geological Characteristics of the X03 Vein

The X03 vein is in the northeastern part of the Jiajika deposit and tectonically in the northeastern margin of the Jiajika structure-magmatic dome, approximately 3 km away from the Majingzi two-mica granite (Figure 2). The X03 vein is large scale, shallow burial, and slow occurrence and can be open pit mined, which is the most valuable development. The veins are covered by the deposits of Quaternary (up to 0.8 m of colluvium and soil) with sporadic outcrops. The ore vein is near the north–south strike and inclined to the west, with dip angles of 25°~35° and a length of more than 1050 m. The average thickness is 66.4 m, and the thickest is 110.17 m (at line 03). At present, the continuing extension of the ore bodies on the south and north sides has not been controlled. The ore body is simple in shape, generally in the shape of lamellar and lenticular bodies, and is a simple branching compound (Figure 3a–c) [29–31].
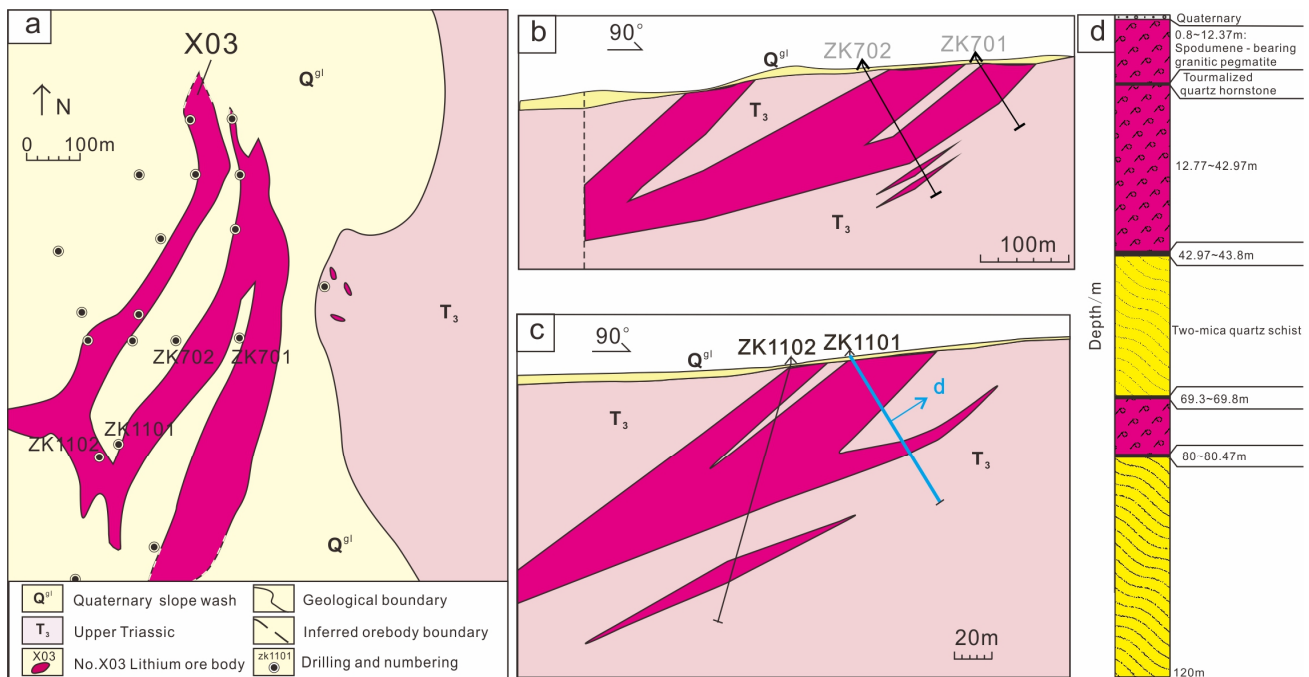
Figure 3. Plane and section geological map of the Jiajika X03 vein in western Sichuan; (**a**) Schematic diagram of plane projection; (**b**) X03 vein in the No.7 exploration line profile diagram, the vein is simple branching compound; (**c**) Profile of exploration line No. 11 of the X03 Vein, the vein presents a simple branching compound; (**d**) ZK1101 lithologic histogram.

Previous studies suggested that the X03 vein was a granite-pegmatite vein with whole-vein lithium industrial mineralization. Through the cataloging of borehole ZK1101, which is a typical borehole, granite-pegmatite can be locally found in the X03 vein, and its ore minerals have been documented [24,32,33]. Borehole ZK1101 is divided into several large layers according to different lithologies, and the core catalog data are as follows (Figure 3d): (1) the first layer occurs from 0 to 0.8 m and is the Quaternary gray residual slope deposit; it is composed of earthen clay, grayish-black mica schist fragments and a few light grayish-white pegmatite fragments; (2) the second layer occurs from 0.8 to 42.97 m and is granitic pegmatite with spodumene mineralization, which is the visible upper layer of the borehole. Between 5.73 to 8.32 m in the upper part of the layer, the granite pegmatite is black, with a relatively uniform composition, and occasionally spodumene veins cut through it. The 12.37~12.77 m layer is tourmaline hornfels; (3) the third layer occurs from 42.97 to 69.8 m and is gray–black garnet that crosses andalusite quartz schist; the top and bottom are superimposed tourmalization surrounding rock alteration; (4) the fourth layer occurs from 69.8 to 80 m, is granitic pegmatite with spodumene mineralization, has lithology that is roughly similar to the upper layer, and is the visible lower layer of the borehole; (5) the fifth layer occurs from 80 to 126.49 m and is gray–black garnet and alusite quartz schist, with tourmalization surrounding rock alteration near the bottom floor of the lower ore layer.

Usually, the rocks surrounding the roof have more developed the tourmalinization than the rocks surrounding the floor, but the most developed tourmalinization occurs in the interlayer in pegmatite. Tourmaline is produced in the surrounding rock edge close to pegmatite, with evident orientation; it is dark brown, needle-like and its contents are 0.5%~5%, with coarse grain size and a diameter that reaches 5 mm Tourmaline is generally replaced by quartz and forms a sieve structure. Most of the tourmaline minerals are black, long columnar, acicular euhedral crystals that are 1~4 mm long, with individual crystals up to 10 mm long, 0.1~0.2 mm in diameter and a large change in the content of approximately 5%~10%. The metasomatism is strong, with tourmalinization as the main process and

biotitization as the secondary process. The minerals, likewise staurolite and andalusite, have disappeared after metasomatism transformation (Figure 4c).
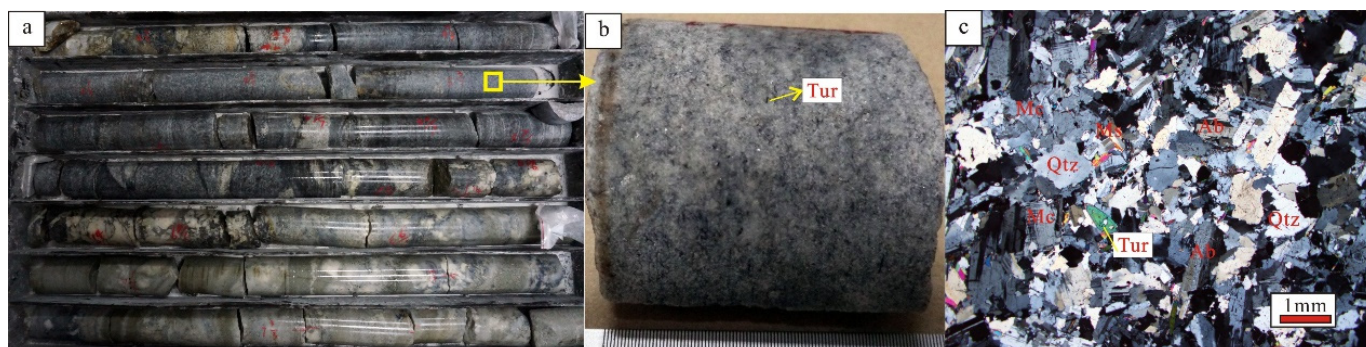

Figure 4. Hand specimen and micrograph photographs of the X03 vein in the ZK1101 tourmaline-bearing granite pegmatite. Ab-albite; Mc-microcline; Qtz-quartz; Tur-tourmaline. (**a**) ZK1101 core image; (**b**) Hand specimen photograph of tourmaline-bearing granite pegmatite; (**c**) Microscopic photomicrograph of tourmaline-bearing granite pegmatite.

2.3. Major Mineral Characteristics of the Jiajika X03 Vein

Mica, feldspar and quartz are the most important petrogenic minerals of granite and granite-pegmatite, and mica and feldspar are often used as important marker minerals to classify pegmatite and indicate its genetic significance. The most important ore mineral in the Jiajika X03 vein is spodumene, and rare metal minerals, such as beryl, are also visible under the microscope. The most common accessory minerals are tourmaline and garnet, and tourmaline often has a high content, which can sometimes reach the content of rock minerals. The following is a description of the most important minerals in the Jiajika X03 vein and the most common minerals in pegmatite.

(1) Muscovite. The muscovite in the Jiajika X03 vein has a white, scaly structure, and the contents are approximately 3%–5%. It has an idiomorphic–hypidiomorphic schistose structure with different diameters (1–5 mm). The muscovite corresponds to structural units of different grain sizes and is often associated with quartz and albite. Near the alteration zone, muscovite in greisen of the marginal facies of granitic rocks appears in a hypidiomorphic schistose structure, with diameters of approximately 0.5~1 mm and large contents of approximately 8%~10% (Figure 5a,b). (2) Garnet. Garnet minerals are produced in both pegmatite and the surrounding rock. Garnet minerals in pegmatite appear in microcrystalline and fine crystalline spodumene structural units, and the distribution is uneven. It has other granular or metasomatic residual structures, the particle sizes are approximately 0.5~1 mm, and the contents are approximately 3%~5%. Some crystal shapes are better, and some are replaced by quartz, feldspar and other minerals. The garnet in schist is a characteristic metamorphic mineral; it is a granulomorphic phenocryst, the particle size is approximately 0.5 mm, and the contents are approximately 3%~5% (Figure 5c,d). (3) Beryl. The beryl produced in the Jiajika X03 vein is milky white in color, generally has a granular shape, and a few have hexagonal columnar shapes; the beryl is few in quantity, is visible in each structural zone containing spodumene, and it is often found near spodumene minerals. Micromineral inclusions are occasionally visible in beryl crystals, which have weak directionality and may be tourmaline (Figure 5e,f).
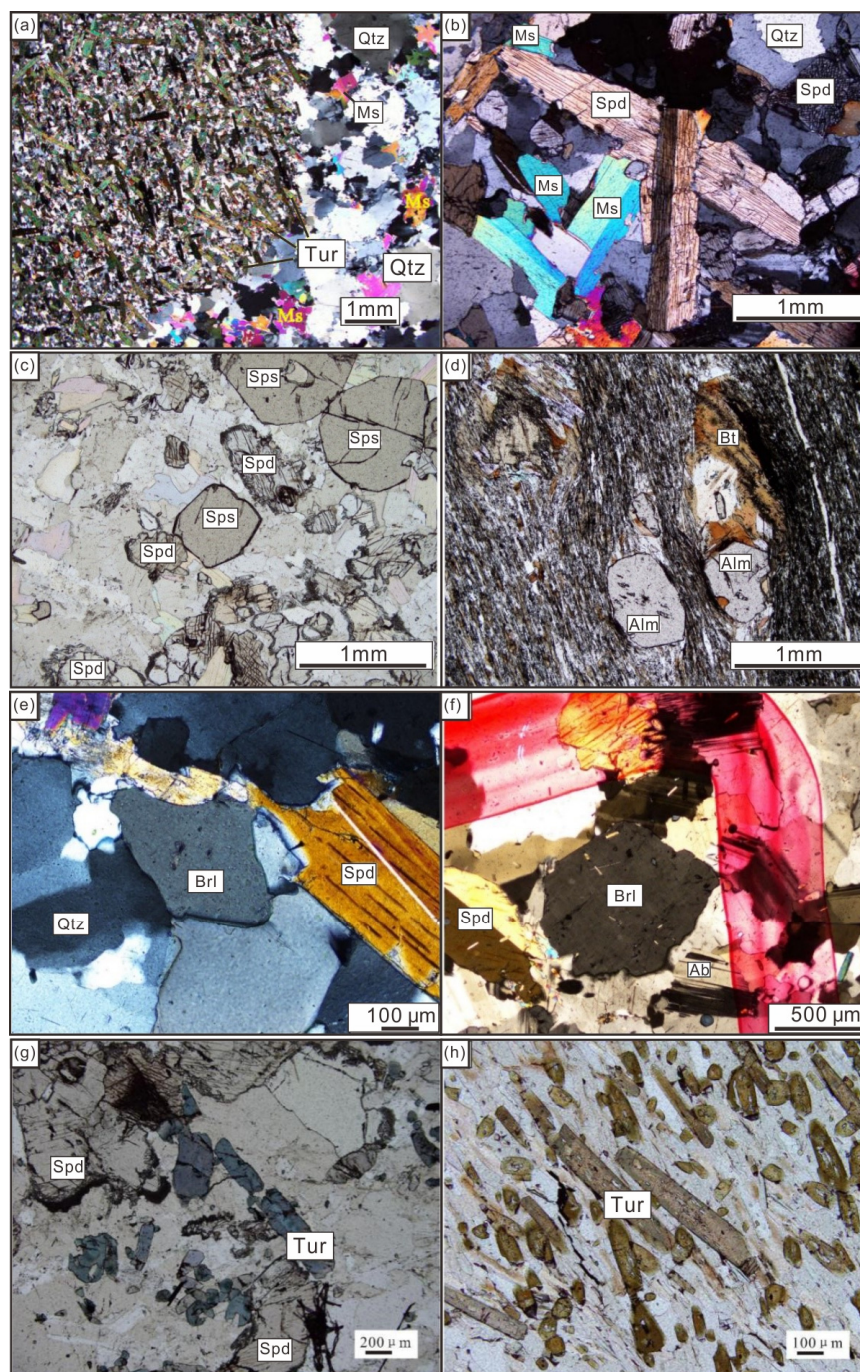
Figure 5. Main mineral characteristics of pegmatite and alteration zone in the Jiajika X03 vein; (**a**,**b**) muscovite; (**c**,**d**) garnet; (**e**,**f**) beryl; (**g**,**h**) Tourmaline; Qtz—quartz; Ms—muscovite; Spd—spodumene; Tur—tourmaline; Sps—spessartite; Alm—almandine; Bt—biotite; Ab—albite; Brl—beryl.

3. Sample Description and Analytical Method

3.1. Sample Description

In this paper, systematic sampling of tourmaline-bearing granite pegmatite, spodumene-bearing granite pegmatite, tourmaline hornfels and two-mica quartz schist from drill hole ZK1101 of the X03 vein is carried out. Tourmaline is a widely distributed accessory mineral in the contact zone between pegmatite and surrounding rock in the Jiajika mining area, as well as in the X03 vein. Based on the color, all are schorl tourmaline, and thus far, no brightly colored tourmaline minerals have been found in the pegmatite in the Jiajika mining area.

The tourmaline in the X03 vein is mostly idiomorphic to hypidiomorphic and fine needle- or column-shaped, with strong pleochroism (colorless blue), central protrusion, color bands and near-parallel extinction (Figure 5g); these features are visible in all structural units. Tourmaline varies in size, with local aggregation and scattered distribution. Produced in coarse-grained quartz and feldspar particles, it crystallizes later and is not replaced by other minerals. The tourmaline content is higher, but the distribution is more disorderly. Some are fine needle-shaped and blue and present as inclusions or occurrences in quartz minerals. A large amount of tourmaline is developed in the tourmaline-altered surrounding rock (tourmaline hornfels). Under the microscope, it is brown, has a fine grain structure, long columnar and needle shapes, euhedral granular sections and is long columnar and longitudinal in plan view (Figure 5g,h). Strong polychromatism (colorless–brown), evident interference colors, and secondary orange red–secondary blue–green colors are observed. Tourmaline often has a sieve structure, and after being metasomatized, it usually contains small particles with quartz inclusions. The arrangement of tourmaline in the alteration zone has strong directivity.

3.2. Analytical Method

The electron probe test of the major elements in tourmaline was carried out at the Institute of Mineral Resources, Chinese Academy of Geological Sciences. The microzone analysis of the samples was carried out with the JXA-8230 electron probe microanalyzer produced by JOEL Electronics Co., Ltd., Tokyo, Japan. The test conditions were as follows: the acceleration voltage was 20 kV, the current was 20 nA, the temperature was 24 °C, and the beam spot diameter was 5 μm. In the analytical test, the Si, Na, and Al contents were calibrated by a jadeite standard sample, the Mg content was calibrated by a magnesium olivine standard sample, the K content was calibrated by a potassium feldspar standard sample, the Ca content was calibrated by a wollastonite standard sample, the Fe content was calibrated by a hematite standard sample, the Ti content was calibrated by a rutile standard sample, the Mn content was calibrated by a standard sample of manganese oxide, and the Cr content was calibrated by a standard sample of chromium oxide.

An in situ test of trace elements in minerals was completed at the Institute of Mineral Resources, Chinese Academy of Geological Sciences on a laser ablation inductively coupled plasma mass spectrometry (LA–ICP–MS) instrument. A Thermo Element II plasma mass spectrometer was used, and the laser ablation system was a New Wave Up213. He was used as the carrier gas for the ablated material in the experiment. The laser wavelength was 213 nm, the beam spot was 40 μm, the pulse frequency was 10 Hz, the energy was 0.176 mJ, and the density was 23–25 J/cm^2. During the test, the laser beam set was initially blocked for 15 s, and then the sample was exposed to the laser for 45 s for continuous ablation. The analysis time of a single point test was 75 s. The measured parameters of plasma mass spectrometry were as follows: the cooling gas flow rate (Ar) was 15.55 L/min; auxiliary gas flow rate (Ar) was 0.67 L/min; the carrier gas flow rate (He) was 0.58 L/min; the sample gas flow rate was 0.819 L/min; and the Rf generator power was 1205 W.

In situ analysis of the boron isotope microregions was performed at the Key Laboratory of Mineralization and Resource Evaluation, Ministry of Natural Resources, Institute of Mineral Resources, Chinese Academy of Geological Sciences. The Neptune LA–multicollector (MC)–ICP–MS and the NewWave Up213 laser ablation system were used. The beam diameter of the laser was 25 μm, the frequency was 10 Hz, the energy density was approximately 8 J/cm^2, and He was used as the carrier gas (0.8 L/min). ^{10}B and ^{11}B were simultaneously analyzed via Faraday Cups L3 and H4, respectively, and LA–MC–ICP–MS sampling was conducted by single-point ablation. Before data analysis, IAEA B4 ($\delta^{11}B$ is $-8.36 \pm 0.58‰$) was used to calibrate the instrument to achieve the optimal state. The internal standard was tourmaline IMR RB1 ($\delta^{11}B$ was $-12.97 \pm 0.97‰$), and the external standard was tourmaline IAEA B4 ($\delta^{11}B$ was $-8.36 \pm 0.58‰$). In the test process, IMR RB1 ($\delta^{11}B$ is $-12.97 \pm 0.97‰$) was measured twice before and after every 4 points to correct the sample, and the accuracy (2σ) was approximately 1‰. Hou et al. [34] describes the detailed process.

4. Results

4.1. Major Elements of Tourmaline

In this study, many electron probe tests (65 points in total) were conducted on 13 tourmaline samples of two-mica quartz schist (Tur-I), tourmaline hornfels (Tur-II), tourmaline-bearing granite pegmatite (Tur-III), and tourmaline-bearing granite pegmatite (Tur-IV) from the drill hole ZK1101 of the X03 vein. The structural formula of tourmaline is $XY_3Z_6(T_6O_{18})(BO_3)_3V_3W$. The structural formulas were calculated on the basis of 31 anions of the tourmaline. B_2O_3, H_2O and Li_2O were calculated on stoichiometry for B = 3 atom per formula unit (apfu), OH + F = 4 apfu and Li = 15−total (T + Z + Y). The range and average mole factions of end-member compositions of the four types of tourmalines are tabulated in Table 1. All data can be found in Supplementary Table S1. Since the analytical results show that $w(Cr_2O_3) < 0.02\%$, $w(SrO) < 0.01\%$, and $w(BaO) < 0.2\%$, these terms were not involved in the calculation of the structural formula of tourmaline. The calculation method used WinTac software (IMA-2011) developed by Yavuz et al. [35].

Table 1. Petrological characteristics of main samples from the borehole (ZK1101) containing the Jiajika X03 vein.
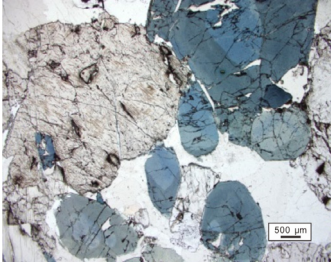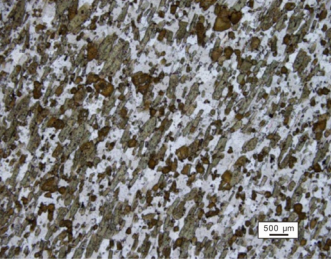
Samples	Petrographic Characteristics	Tourmaline Characteristics	Photomicrographs
Spodumene-bearing granite pegmatite	The rock is gray–white and has medium–fine granitic blocky structures. The main minerals are spodumene (10%~20%), albite (25%~35%), quartz (35%~45%), partially visible garnet and tourmaline (1%~3%). The mineral particle size changes to a certain extent. The spodumene is approximately 0.5 mm in length, with a fine-grained texture, up to 5 cm in length, and approximately 2~5 mm in width, with a coarse-grained texture.	Tourmaline is blue and hypidiomorphic granular; the interference color for the first level is yellow, larger particles have visible colored rings, and it often appears with spodumene.	
Tourmaline-bearing granite pegmatite	It has gray–black mixed with gray–white spotted structures. The main minerals are albite (30%~40%), quartz (35%~45%), and tourmaline (5%~8%); the overall composition is more uniform; the tourmaline content is high; and spodumene is barely visible.	Tourmaline has an acicular or granular texture, it is colorless–green–blue, shows strong pleochroism, has parallel extinction, exists in coarse quartz and feldspar particles, and is not replaced by other minerals.	
Two-mica quartz schist	The schist has a porphyroblastic texture and a schistose structure, with a certain silky luster on the surface. The matrix is a flaky fine-grained structure and is mainly composed of biotite and quartz. The phenocrysts are mainly staurolite with irregular particle sizes of approximately 2~3 mm.	Tourmaline has a fine-grained structure; with euhedral granular sections; and is long, columnar and longitudinal in plan view; it is green and brown and has strong pleochroism. The tourmaline contains quartz inclusions and has a diablastic texture.	

Samples	Petrographic Characteristics	Tourmaline Characteristics	Photomicrographs
Tourmaline hornfels	It is grayish black, gray or brown, homogeneous or slightly crystalline, with shell-like fractures. Quartz is the main mineral (40%~60%), followed by potassium feldspar (15%~25%), plagioclase (5%~15%), biotite (1%~2%), tourmaline (1%), etc.	Tourmaline is distributed in the rock in the form of idiomorphic–hypidiomorphic schistose textures, with filiform or granular structures, and may also exist in the form of fissure filling.	
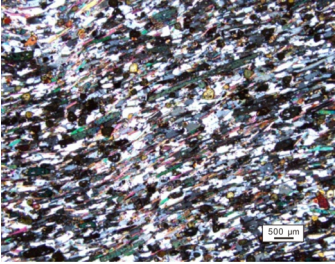
According to Ca, Na+K and X-site vacancies in the lattice of tourmaline, tourmaline can be divided into three categories: alkaline tourmaline, calcium tourmaline and X-site vacancy tourmaline. Then, it is further subdivided according to the distribution of the elements in positions V, W, Y and Z [36,37]. The calculation results from the apfu values based on the probe data show that the X-site vacancy elements of tourmaline studied in this paper are mainly Na and K, and all categories are alkalic group, Tur-II, Tur-III and Tur-IV are Oxy species–Fluor species tourmaline, and Tur-I is Hydroxy species tourmaline (Figure 6a,b). According to the classification diagram of tourmaline (Figure 6c–e), Tur-III and Tur-IV are schorl tourmaline, Tur-Iare dravite tourmaline, and Tur-II are foitite tourmaline. In summary, the tourmaline in the Jiajika X03 vein are classified as schorl–Oxy/Fluor–schorl, dravite–Hydroxy-dravite and foitite–Oxy foitite solid solutions [30]. In the Al-Fe-Mg and Ca-Fe-Mg ternary diagrams of Henry and Guidotti [38], the Tur-III and Tur-IV type tourmaline plots in the field 2 and the Tur-I and Tur-II type tourmaline falls in the field 5 and 10 (Figure 7a,b).
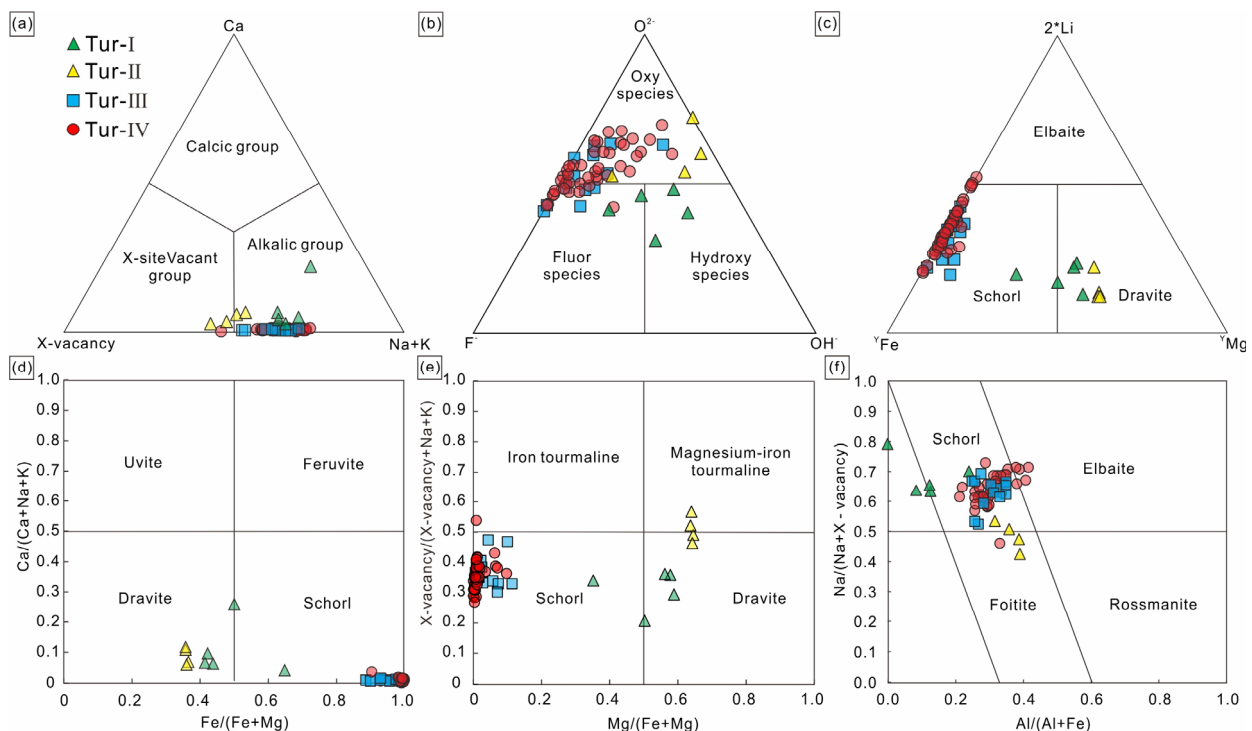

Figure 6. Classification diagrams for tourmalines [36], (**a**) Ca-X-site vacancy-Na + K diagrams; (**b**) O^{2-}-F^--OH^- (W-site) diagrams; (**c**) Li-Fe-Mg diagrams, (**d**) calculated Fe/(Mg + Fe) versus Ca/(Na + Ca + K), (**e**) Mg/(Mg + Fe) versus X-site vacancy/(X-vacancy + Na + K), (**f**) Al/(Al + Fe) versus Na/(Na + X-vacancy).
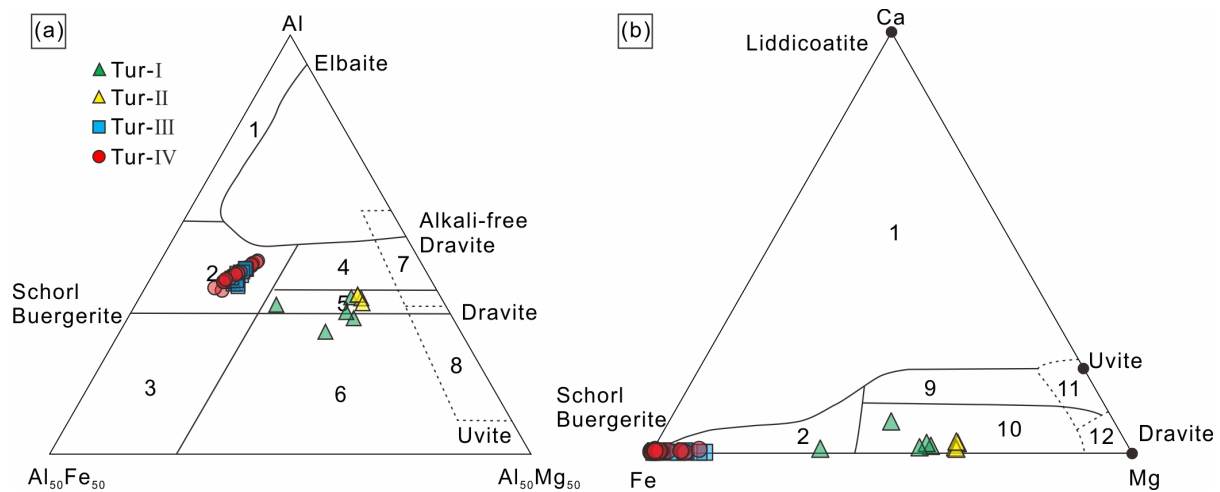
Figure 7. Ternary Al–Fe-Mg (**a**) and Ca–Fe-Mg (**b**) diagrams showing compositional variations of tourmalines from the Jiajika X03 vein. The regions define the compositions of tourmaline based different rock types, according to [38]. 1 = Li–rich granitoids and associated pegmatites and aplites; 2 = Li–poor granitoids and associated pegmatites and aplites; 3 = Fe^{3+}–rich quartz–tourmaline rocks (hydrothermally altered granites); 4 = Metapelites and metapsammites coexisting with an Al-saturating phase; 5 = Metapelites and metapsammites not coexisting with an Al–saturating phase; 6 = Fe^{3+}–rich quartz–tourmaline rocks, calc silicate rocks, and metapelites; 7 = Low Ca metaultramafics and Cr, V–rich metasediments; 8 = Metacarbonates and metapyroxenites; 9 = Ca–rich metapelites, metapsammites, and calc-silicate rocks; 10 = Ca–poor metapelites, metapsammites, and quartz–tourmaline rocks; 11 = Metacarbonates; 12 = Metaultramafics.

The Tur-III and Tur-IV tourmalines have similar major element compositions, containing high FeO contents (Tur-III, 10.90%–12.90%; Tur-IV, 9.90%–13.55%) and low MgO contents (Tur-III, 0.15%–0.59%; Tur-IV, 0.20%–0.78%). The Tur-III and Tur-IV tourmalines have high Al_2O_3 contents (Tur-III, 33.48%–35.45%; Tur-IV, 32.93%–36.48%). The Tur-II tourmalines have lower FeO contents (5.84%–6.18%) and higher MgO contents (Tur-I, 5.34%–5.82%; Tur-II, 5.81%–6.20%). The four types of tourmalines have similar vacancies in the X-site (0.16–0.56). According to the classification of Henry et al. (2011) [36] based on the X-site occupancy, all four types of tourmaline belong to the alkalic group (Figure 6a). The four tourmaline types display large variations in Mg/(Mg + Fe) ratios from 0.00 to 0.64 (Table 2). The Tur-I and Tur-II tourmaline types have higher CaO contents (0.16%–1.24%) and lower Na/(Na + Ca) ratios than the other two types. All tourmaline samples show minor contents of MnO (0.00%–0.78%), TiO_2 (0.00%–1.05%) and K_2O (0.00%–0.06%).

Figure 8 shows plots of all tourmaline analyses with various substitution vectors as references. All tourmaline samples have a trend corresponding roughly to the $MgFe_{-1}$ vector, with a small contribution of the $FeAl_1$ exchange vector in the Tur-III and Tur-IV samples. All values of $\sum(Mg + Fe) < 3$ apfu and total Al > 6 apfu indicate that there is considerable Al (up to 1.03 apfu) in the Y-site (Figure 8a) with a combination of the foitite $((Na, Mg) (^X\square, Al)_{-1})$ and olenite $((Mg, OH) (Al, O)_{-1})$ substitution vectors (Figure 8b,c). Additionally, the contribution of the substitution vector $(Ca, Mg_2) (^X\square, Al_2)_{-1}$ (Figure 8d) can explain the variation in Ca in the Tur-I and Tur-II samples (0.002–0.22 apfu).

Table 2. Major element compositions of tourmalines from the Jiajika X03 vein.

Type		Tur-I N = 5			Tur-II N = 4			Tur-III N = 13			Tur-IV N = 43		
		Range	Mean	SD	Range	Mean	SD	Range	Mean	SD	Range	Mean	SD
SiO_2		36.63–38.08	37.33	0.59	37.26–38.75	37.80	0.58	35.59–37.42	36.70	0.51	35.66–38.07	36.91	0.54
TiO_2		0.75–1.05	0.86	0.11	0.39–0.81	0.61	0.17	0.07–0.36	36.70	0.51	0.00–0.29	0.11	0.06
Al_2O_3		30.53–33.03	31.89	0.81	33.53–34.81	34.23	0.51	33.48–35.45	0.16	0.08	32.93–36.48	34.51	0.77
V_2O_3		0.00–0.07	0.05	0.02	0.00–0.10	0.06	0.04	0.00–0.09	34.32	0.58	0.00–0.12	0.01	0.02
FeO		7.32–11.02	8.60	1.41	5.84–6.18	6.05	0.13	10.90–12.90	0.04	0.03	9.90–13.55	11.90	0.97
MnO		0.02–0.16	0.08	0.05	0.00	0.00	0.00	0.15–0.59	11.98	0.63	0.20–0.78	0.41	0.11
ZnO		0.00–0.08	0.03	0.03	0.00–0.08	0.03	0.03	0.24–0.54	0.35	0.12	0.32–0.75	0.49	0.10
MgO		3.34–5.82	5.17	0.93	5.81–6.20	6.02	0.15	0.03–0.91	0.42	0.11	0.00–0.74	0.10	0.15
CaO		0.16–1.24	0.46	0.40	0.16–0.38	0.27	0.09	0.01–0.05	0.32	0.29	0.00–0.09	0.04	0.02
Na_2O		1.88–2.11	1.96	0.08	1.34–1.59	1.48	0.09	1.60–2.10	0.03	0.01	1.43–2.22	1.97	0.15
K_2O		0.01–0.03	0.02	0.01	0.01–0.03	0.02	0.01	0.02–0.06	1.92	0.15	0.00–0.05	0.03	0.01
F		0.19–0.50	0.32	0.11	0.00–0.40	0.14	0.16	0.14–0.82	0.03	0.01	0.11–0.78	0.46	0.17
Li_2O *		0.27–0.57	0.44	0.10	0.24–0.48	0.31	0.10	0.36–0.87	0.52	0.16	0.33–1.17	0.68	0.19
H_2O *		2.92–3.20	3.08	0.09	2.97–3.14	3.08	0.07	2.56–2.94	0.61	0.17	2.54–2.96	2.78	0.09
B_2O_3 *		10.48–10.72	10.63	0.11	10.75–10.98	10.85	0.09	10.38–10.57	2.76	0.09	10.30–10.73	10.49	0.08
O=F *		0.08–0.21	0.13	0.05	0.00–0.17	0.06	0.07	0.06–0.35	10.46	0.05	0.05–0.33	0.20	0.07
Total *		100.79–101.38	101.05	0.22	100.41–101.79	101.02	0.61	100.16–102.04	0.22	0.07	99.81–103.63	101.09	0.73
T-site	Al	0.00	0.00	0.00	0.00	0.00	0.00	0.00–0.04	0.00	0.01	0.00–0.08	0.00	0.01
	Si	6.02–6.17	6.11	0.06	6.02–6.13	6.06	0.05	5.96–6.20	6.10	0.07	5.92–6.29	6.12	0.08
Z-site	Al	5.96–6.00	5.99	0.02	6.00	6.00	0.00	6.00	6.00	0.00	6.00	6.00	0.00
	Fe^{2+}	0.00	0.00	0.00	0.00	0.00	0.00	0.00	0.00	0.00	0.00	0.00	0.00

Table 2. *Cont.*

Type		Tur-I N = 5			Tur-II N = 4			Tur-III N = 13			Tur-IV N = 43		
		Range	Mean	SD	Range	Mean	SD	Range	Mean	SD	Range	Mean	SD
Y-site	Al	0.00–0.32	0.16	0.11	0.39–0.52	0.46	0.05	0.58–0.87	0.72	0.10	0.51–1.03	0.74	0.11
	Ti	0.09–0.13	0.11	0.01	0.05–0.10	0.07	0.02	0.01–0.05	0.02	0.01	0.00–0.04	0.01	0.01
	Fe^{2+*}	0.99–1.53	1.18	0.21	0.77–0.84	0.81	0.02	1.52–1.80	1.67	0.09	1.36–1.89	1.65	0.14
	Mn	0.003–0.02	0.01	0.01	0.00	0.00	0.00	0.02–0.08	0.05	0.02	0.03–0.11	0.06	0.02
	Mg	0.83–1.41	1.25	0.22	1.37–1.49	1.44	0.05	0.01–0.23	0.08	0.07	0.00–0.19	0.03	0.04
	Zn	0.001–0.01	0.00	0.00	0.00–0.01	0.00	0.00	0.03–0.07	0.05	0.01	0.04–0.09	0.06	0.01
	Li	0.18–0.37	0.29	0.07	0.16–0.30	0.20	0.06	0.24–0.58	0.41	0.11	0.22–0.78	0.45	0.12
X-site	Ca	0.03–0.22	0.07	0.22	0.03–0.07	0.05	0.02	0.002–0.009	0.01	0.002	0.00–0.016	0.007	0.003
	Na	0.59–0.66	0.02	0.66	0.41–0.50	0.46	0.03	0.52–0.68	0.62	0.05	0.46–0.71	0.63	0.05
	K	0.003–0.006	0.001	0.006	0.002–0.006	0.005	0.002	0.004–0.012	0.01	0.003	0.00–0.01	0.006	0.002
	vacancy	0.16–0.35	0.07	0.35	0.43–0.56	0.49	0.05	0.302–0.473	0.37	0.05	0.27–0.54	0.36	0.05
V+W-site	OH	3.23–3.46	0.09	3.46	3.17–3.37	3.29	0.08	2.84–3.25	3.06	0.10	2.81–3.30	3.07	0.11
	O	0.37–0.54	0.07	0.54	0.57–0.72	0.63	0.06	0.55–0.75	0.67	0.06	0.52–0.80	0.69	0.06
	F	0.10–0.26	0.06	0.26	0.00–0.20	0.07	0.08	0.07–0.43	0.27	0.09	0.06–0.41	0.24	0.09

SD: standard deviation; *: calculated.
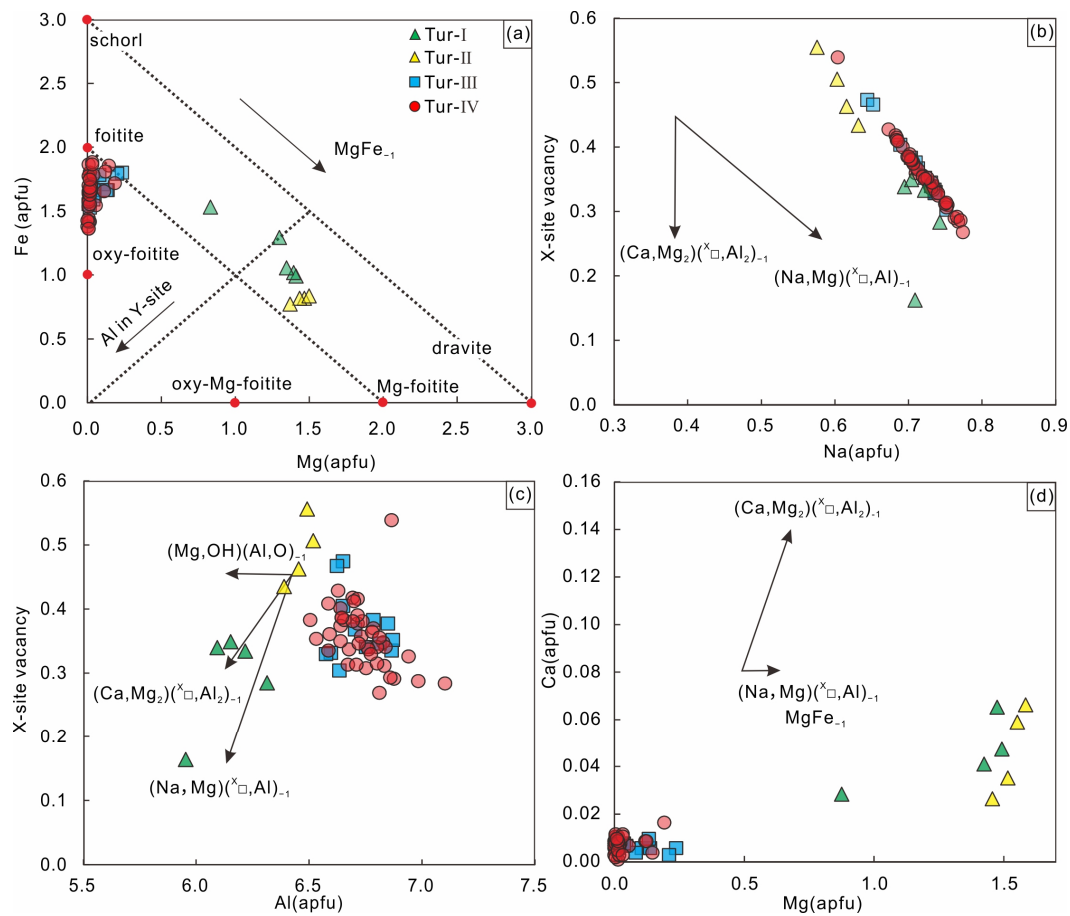
Figure 8. (**a**) Plot of Mg versus Fe, (**b**) Plot of Na versus X-site vacancy, (**c**) Plot of Al versus X-site vacancy, (**d**) Plot of Mg versus Ca of cation occupancies in tourmalines from the Jiajika X03 vein with common exchange vectors as reference. All values are in apfu.

4.2. Trace Elements of Tourmaline

The LA-ICP-MS trace element analysis data selected in this paper are listed in Supplementary Table S1. Most trace elements have concentrations below 10 ppm. Concentrations of Li, Zn, Ti, and Mn are high (tens to hundreds of ppm), while Mo, Cs, Cd, Zr, As, Y, and most rare earth elements (REEs) are low (<1 ppm). Some trace elements vary by orders of magnitude, especially As (0.00~19.76 ppm) and Pb (0.00~14.85 ppm).Compared with schorl (Tur-III and Tur-IV), dravite (Tur-I) and foitite (Tur-II) in the Jiajika X03 vein has lower Li contents (96×10^{-6}~156×10^{-6}) and Mn contents (132.06×10^{-6}~670.01×10^{-6}). Its contents of Mg (4071.04×10^{-6}~$41,228.56 \times 10^{-6}$), Ti (2247.07×10^{-6}~5737.79×10^{-6}), Pb ($283,197.04 \times 10^{-6}$~$411,786.23 \times 10^{-6}$), V ($190.86 \times 10^{-6}$~$349.50 \times 10^{-6}$), Sr ($9.23 \times 10^{-6}$~$160.28 \times 10^{-6}$) and Sc ($10.17 \times 10^{-6}$~$34.27 \times 10^{-6}$) were high, and the contents of Zn (9×10^{-6}~284×10^{-6}) were significantly low. The dravite and foitite tourmaline has similar Cu, Ga, Y and Sn contents to schorl tourmaline.

4.3. Boron Isotopic Compositions of Tourmaline

The boron isotopic compositions of tourmaline in this study are shown in Supplementary Table S1. The $\delta^{11}B$ values of various types of tourmalines ranges from -11.47‰ to -4.93‰, with a Gaussian distribution around -12‰ (Figure 9a,b). The $\delta^{11}B$ values of the Tur-I tourmaline are -7.09‰ to -5.17‰ (12 analyses from 5 samples), the $\delta^{11}B$ values of the Tur-II tourmaline are -7.00‰ to -4.93‰ (13 analyses from 4 samples), the $\delta^{11}B$ values of the Tur-III tourmaline are -9.46‰ to -7.35‰ (4 analyses from 1 sample), and the $\delta^{11}B$ values of the Tur-IV tourmaline are -11.47‰ to -7.48‰ (65 analyses from 17 samples). The isotopic zonation of the Tur-I, Tur-II and Tur-III tourmaline particles can be neglected,

but the isotopic zonation of Toure-IV tourmaline particles is obvious. From the rim to the core, the $\delta^{11}B$ value generally decreases from 8.05 ‰ to 10.14 ‰ (Figure 10).
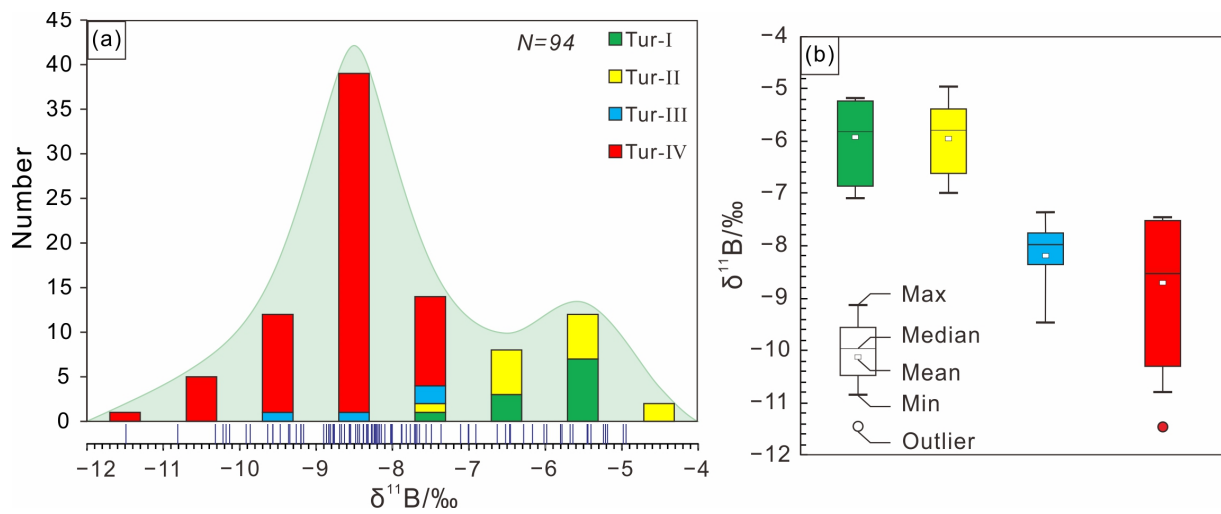

Figure 9. (**a**) Frequency histogram of boron isotopic compositions ($\delta^{11}B$) of tourmalines from the Jiajika X03 vein. (**b**) Box-whisker plots showing comparisons of boron isotope of tourmalines from the Jiajika X03 vein.
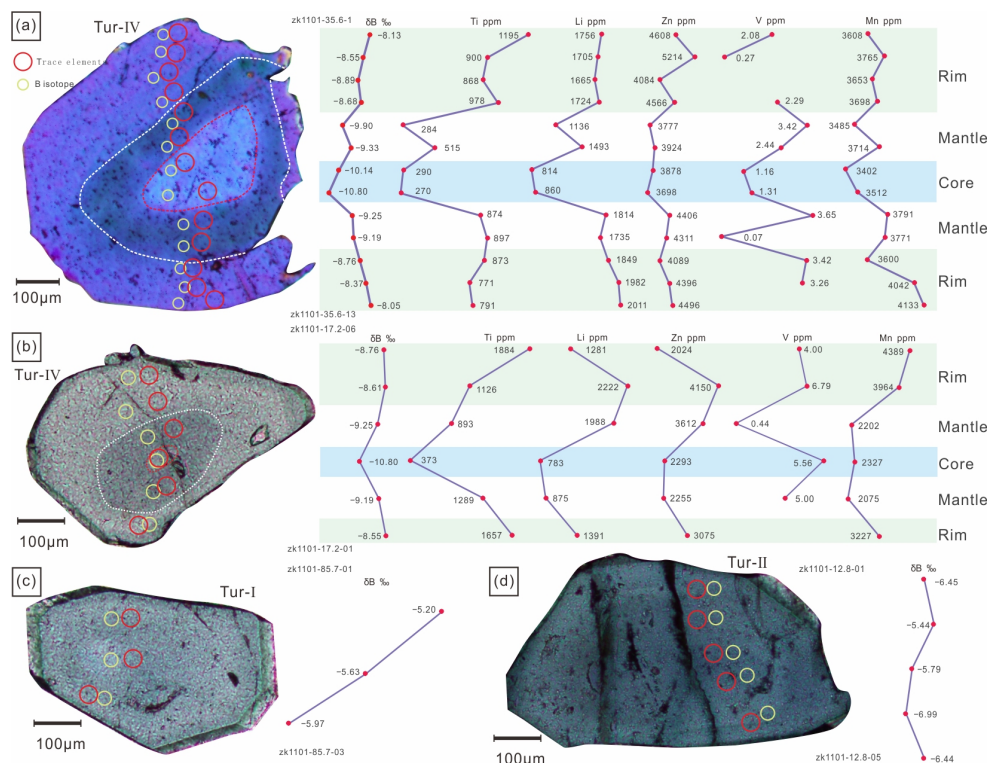

Figure 10. Trends of trace elements and boron isotopes in different types of tourmaline. (**a**) Sample ZK1101-35.6; (**b**) Sample ZK1101-17.2; (**c**) Sample ZK1101-85.7; (**d**) Sample ZK1101-12.8.

5. Discussion

5.1. Origin of Tourmaline

The chemical composition of tourmaline can vary due to several factors, such as host rock lithology, coexisting mineral assemblage, fluid composition, and P–T–fO$_2$ conditions (where P, T, and fO$_2$ are pressure, temperature, and oxygen fugacity, respectively). These

factors have been identified in previous studies to play a role in shaping the chemical makeup of tourmaline [38–43]. Tourmaline is a ubiquitous boron-rich mineral in the Jiajika deposit, mainly developed in the pegmatite, granite surrounding rock and alteration zones of the X03 vein (Tur-I to Tur-IV). The X03 tourmaline vein at Jiajika provides crucial information for understanding the evolution of the magmatic-hydrothermal system in the area. Researchers have used the petrographic and textural features of the vein, along with its elemental and isotopic data, to reconstruct the magmatic evolution model. The tourmaline found in the vein is either blue-green or khaki in color, and lacks finescale zonation. Furthermore, the Tur-III and Tur-IV tourmalines in the vein are primarily schorl, while Tur-I and Tur-II tourmalines are dravite and foitite. The Tur-III and Tur-IV type tourmalines also show similar trace element patterns and B-isotopic compositions (Figure 9). The Tur-III and Tur-IV type tourmalines have high aluminum contents at the Y site (Al^Y = 0.51–1.03 apfu), and the Tur-I and Tur-II type tourmalines have lower aluminum contents at the Y site (Al^Y = 0.00–0.52 apfu).

Previous studies suggested that magma-derived tourmaline has a high Al content at Y-site, while hydrothermal tourmaline has a poor or low Al content [44]. These characteristics of tourmaline are similar to those of magmatic tourmalines described by London et al. [45]. Therefore, we believe that the Tur-III and Tur-IV type tourmalines from the Jiajika X03 vein are mainly derived from magmatic and that the Tur-I and Tur-II type tourmalines are mainly derived from hydrothermal fluids.

The late-crystallizing magmatic tourmaline (Tur-III and Tur-IV) is commonly found in a homogenous texture between quartz and plagioclase (Figure 5g,h). Its chemical composition is relatively consistent, with a high Fe/(Fe + Mg) (0.89–1.00) and Na/(Na + Ca) (0.97–1.00) ratio, making it a member of the schorl series. The tourmaline's Fe-Al-rich feature, with Fe and Al apfu ranging from 1.36–1.89 and 6.51–7.11, respectively, reflects the overall bulk composition of the granites where it is found. These granites are typically peraluminous (with A/CNK mostly ≥1.0) and have high $FeO^T/(FeO^T + MgO)$ ratios of 0.93–1.00 [46]. These textural and chemical features are consistent with a primary magmatic origin [44,47,48].

While the Zn content in Tur-IV tourmaline (>200 ppm) from Jiajika is not as high as some Zn-bearing tourmalines (ZnO > 1 wt%) [49,50], it is higher than most normal tourmalines (<100 ppm) (Figure 11d) [51,52]. It is suggested that the enrichment in Zn is due to the dissolution of gahnite by fluid containing Na, Li, F, B, and Be, followed by reprecipitation [50]. This can explain the presence of Zn-rich tourmaline rims found in the samples. Zn has low distribution coefficient values in silicate melt and is expected to partition into the aqueous fluid during fractionation [53,54], resulting in the precipitation of Zn-rich tourmalines. Zn can also easily transfer from strata to fluid/melt, which potentially causes the high Zn content of Tur-IV tourmaline in Jiajika [55], as Zn has high mobility in fluids.

Hydrothermal tourmaline exhibits characteristic oscillatory zoning and systematic chemical variation at the growth-band scale. Such features can reflect either rapid tourmaline growth or episodic physicochemical changes (e.g., P–T-X-fO_2) in the hydrothermal system [56,57]. According to research, the differences in chemical composition between Tur-I and Tur-II tourmalines in the Jiajika granite are mainly due to varying degrees of water-rock interaction. Biotite decomposition during greisenization results in relatively low Fe/(Fe + Mg) ratios (0.36–0.65 apfu), which are associated with Tur-I and Tur-II tourmalines. The destruction of biotite also causes Ti leaching from the host granite, which may explain the high Ti content observed in the tourmalines (Supplementary Table S1, Figure 11h). The Ti activity in the magma-hydrothermal transition system may also contribute to the high levels of Ti in Tur-I and Tur-II tourmalines [58,59]. In addition, the Ca and Sr content in the tourmalines is related to feldspar dissolution (Supplementary Table S1, Figure 11e), while lower transition metal content, such as Zn, is likely associated with sulfide precipitation. Consequently, the Tur-I and Tur-II tourmalines are likely precipitated from

magmatic-hydrothermal fluids that were exsolved from the differentiated melt periodically with different chemical compositions determined by varying water/rock ratios.
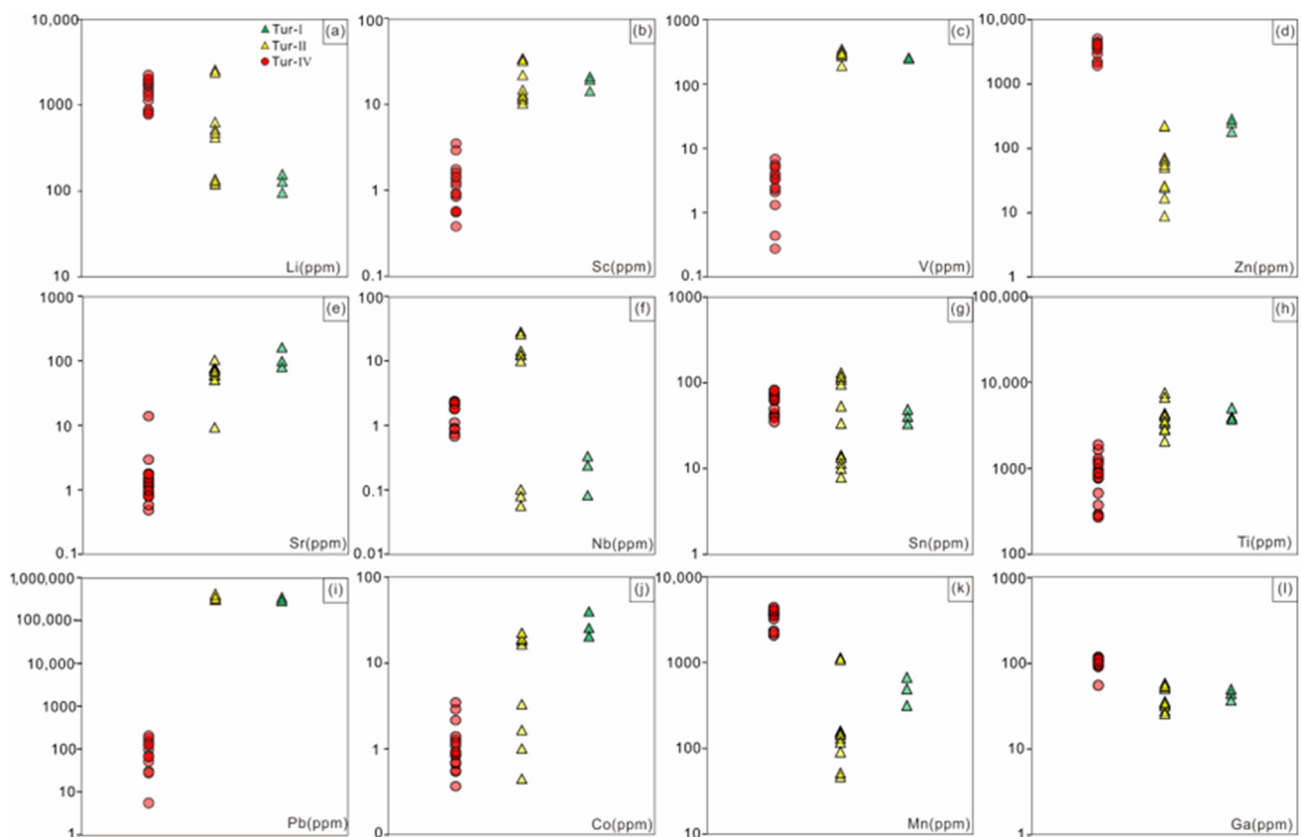

Figure 11. Scatter diagram plots showing comparisons of representative elements in tourmaline from the Jiajika X03 vein. (**a**) Li elements; (**b**) Sc elements; (**c**) V elements; (**d**) Zn elements; (**e**) Sr elements; (**f**) Nb elements; (**g**) Sn elements; (**h**) Ti elements; (**i**) Pb elements; (**j**) Co elements; (**k**) Mn elements; (**l**) Ga elements.

5.2. B Source and Variation

Tourmalines found in pegmatites typically have either magmatic or hydrothermal origins, and differentiating between the two can be challenging based on the characteristics of main and trace elements alone [4,5,13]. Previous research has demonstrated the utility of B isotope compositions in distinguishing between tourmalines of magmatic and hydrothermal origin in pegmatite [5]. Tourmaline boron isotopic compositions are affected by a variety of factors, including source composition [60], isotopic fractionation during boron coordination in coexisting phases, and fluid-rock interactions during fluid evolution [51,60,61]. Boron has a broad isotopic fractionation range spanning from −26.8 to +35‰, making tourmaline boron isotopic compositions a useful tool for examining element sources, fluid-rock interactions, and fluid evolution. Isotopic zonation in magmatic-hydrothermal systems is typically attributed to isotopically distinct sources, fluid boiling, or Rayleigh fractionation [9,52,62–64]. Rayleigh fractionation is caused by continuous tourmaline precipitation, leading to a gradual depletion of boron in the residual fluid, resulting in an ongoing evolution in boron isotopic compositions of both the fluid and tourmaline [60]. In magmatic systems, late-stage magmatic tourmalines have lower $\delta^{11}B$ values due to boron depletion in the remaining melt after tourmaline precipitation [65,66]. Conversely, in hydrothermal systems, continuous tourmaline precipitation can induce Rayleigh fractionation, leading to heavy boron enrichment in late-stage fluids and related tourmaline [66,67].

The $\delta^{11}B$ values of tourmalines from the Jiajika X03 vein surrounding rock and pegmatites are much lower than those of seawater and mantle-derived oceanic crust, but

similar to those of the continental crust (Figure 12) [62,68–70], suggesting a continental crustal origin. This is also in agreement with the source of the host rocks. The Fe-rich and Al-rich nature (Table 2 and Figure 6d,e) of tourmalines compare well with the low Mg/(Fe + Mg) and peraluminous nature of whole-rock compositions of the host rocks (see data in Hou et al.) [71]. In fact, both the surrounding rock and the pegmatites also have peraluminous mineral assemblages such as tourmaline, beryl, garnet and muscovite (Figure 5), indicating that they were derived from sedimentary rocks within the continental crust [61]. The Jiajika X03 vein Li deposits exhibit a narrow range of $\delta^{11}B$ values (95% of values between −10 and −5‰) (Figure 8), attributed to the metasedimentary source of S-type granitic rocks [60]. Tourmaline $\delta^{11}B$ values from the Jiajika X03 vein suggest that boron involved in tourmaline formation is mainly derived from differentiated granites sourced from metasedimentary rocks. This observation is consistent with the peraluminous character of the Majingzi granite, indicating that it is an S-type granite mainly derived from metasedimentary source rocks [19,46,71]. The $\delta^{11}B$ value ranges for tourmaline in IOCG deposits within Copiapó (Chile) [72] and Yerington (USA) are mostly identical (−7.5‰ to +4.2‰ and −5‰ to +5‰, respectively) for deposits associated with S-type granite [73]. Tourmaline $\delta^{11}B$ values from other deposits include quartz-cassiterite veins (−10‰ to −8‰) and quartz-wolframite-cassiterite-Li mica veins (−7.3‰ to −5.2‰) in the Cligga Head Sn–W deposit and $\delta^{11}B$ values of −13.9‰ to −12.0‰ in the Baotan Sn deposit [74]. The boron isotopes within the S-type magma light isotope labeling (average $\delta^{11}B = -11$‰) result from the preferential absorption of ^{10}B by mica and clay, according to Trumbull et al. [51].
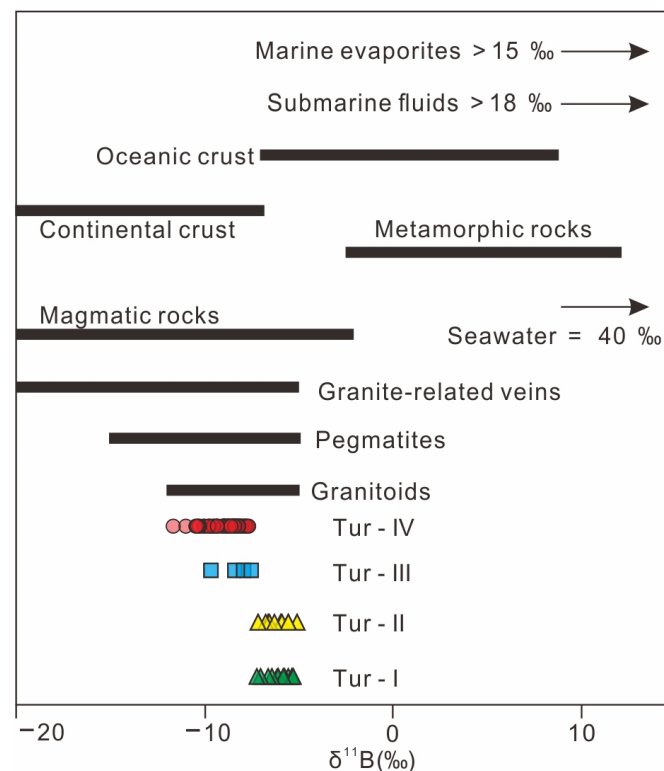

Figure 12. Boron source of the Jiajika X03 vein tourmalines. Ranges of boron isotopes of tourmaline from granite, pegmatite [68], continental crust [62,69] and the other various reservoirs [70] in nature are shown for comparison.

Normally, the $\delta^{11}B$ values of magmatic tourmalines should be similar to those of the parental magma. As exsolved fluids become enriched with ^{11}B during magmatic evolution and degassing, hydrothermal tourmalines display an increase in $\delta^{11}B$ ratios [1]. As a result, the $\delta^{11}B$ variation observed in tourmalines from the Jiajika X03 vein suggests that these

minerals recorded the boron isotopic signatures of the granite magma because boron was quantitatively incorporated into the tourmaline [73]. There are no remarkably compositional differences between the tourmaline cores and rims as well as their boron isotopic compositions in the Jiajika X03 vein tourmaline-quartz veins. This observation is well compatible with the formation of the tourmalines during a single magmatic-hydrothermal stage, with boron-rich fluids being exsolved from the granitic melt. If tourmaline was formed during magmatic stage, a remarkable boron isotope fractionation between the early- and late-stage tourmalines would be observed. Therefore, we conclude that boron in the tourmalines of surrounding rock and pegmatite in the Jiajika X03 vein was probably derived from the Majingzi two-mica granite, which is induced by the partial melting of the metasedimentary precursor, and the tourmaline was formed during the magmatic-hydrothermal process related to granite magmatism.

The $\delta^{11}B$ values of tourmalines from Tur-I to Tur-IV show that melt-tourmaline and melt-fluid fractionation of boron isotopes depend on temperature and the proportion of trigonal to tetrahedral coordination sites of boron. The Jiajika granite's crystallization temperature is around 520 °C [71], and previous studies on natural melts suggest that boron was present in mixing trigonal-tetrahedral coordination sites [4,75–77]. The Rayleigh fractionation effects lead to the progressive depletion of ^{11}B in the residual melt, resulting in $\delta^{11}B$ values of ~–13.27‰ during magmatic tourmaline crystallization [66,67]. Meyer et al. [66] suggested that the fractionation observed in Palmer et al.'s study reflected Rayleigh fractionation effects in experiments on the fractionation of boron between fluid and tourmaline using low B fluids. According to the fractionation values of Meyer et al., the equilibrium Δfluid-tur fractionation factor at 500 °C is −1.8‰. This indicates that the primary magma's $\delta^{11}B$ value was near −6.73‰, similar to the global $\delta^{11}B$ value (−11 ± 4‰) of S-type granites [78]. The difference in $\delta^{11}B$ values between the cores (−10.14‰ and −10.80‰) and rims (−8.05‰ and −8.55‰) of Tur-IV tourmalines could be explained by progressive fractionation between fluid and tourmaline [63,66], as the fluid was enriched in heavy boron after the precipitation of tourmaline (Figure 10a,b).

5.3. Metallogenic Significance of Tourmaline from the Jiajika X03 Vein

Previous studies have shown that as the degree of crystal differentiation of pegmatite increases, the major and trace elements and B isotopic compositions of tourmaline indicate certain changes [4,5]. According to the characteristics of trace elements in the Jiajika X03 vein Tur-IV tourmaline belt, the contents of Ti and Mn in tourmaline gradually increase from the core to the edge of a single pegmatite, while the content of V basically does not change [79–81]. Tur-I and Tur-II tourmaline show no evident ring development, and the chemical composition from the core to the edge has no apparent change. Compared with Tur-I and Tur-II tourmaline, Tur-IV tourmaline is significantly rich in Li, Zn, Ga and Mn, the contents of V, Sr, Ti and Pb are very low, and the contents of Mn and Zn are positively correlated with the contents of Li (Figures 10 and 11). The concentration of Zn is strongly correlated with the nature of the formation environment. The fact that Zn is considered highly mobile in the presence of a fluid phase may, in part, explain its enrichment during fluid exsolution leading to the lithium mineralized pegmatite formation [82]. The amount of Sr in tourmaline nonmineralized environments is consistently high compared to tourmaline in lithium mineralized environments, a feature ascribed to the suppression of plagioclase crystallization in tandem with fractionation of amphibole ± garnet in the lower crust [83–85]. In terms of the tourmaline supergroup minerals (TSM) from unmineralized settings, Pb concentrations are significantly higher, with TSM from granitic pegmatites, for example, averaging 337,490 ppm. The incorporation of Pb into TSM is linked to the Pb availability and competition with other crystallizing minerals, most importantly alkali feldspars and sulfides, which both have high affinities for Pb, with $D_{feldspar}/melt$ = 0.989–2.72 and $D_{sulfide\ melt/silicate\ melt}$ = 140–3300 [86,87]. Gallium has an average concentration in the Earth's upper continental crust of 17.5 ppm [88]. Studies of Ga in natural melts and fluids show that the highest concentrations are associated with fluids of magmatic origin [89]

even though Ga relative to Al concentrations have been shown to increase during fractionation [90]. The concentration of Ga in TSM has been shown to be useful for separating magmatic and hydrothermal samples, with hydrothermal grains having lower concentrations [91]. This is consistent with our actual test results. The magmatic tourmaline (Tur-IV) Ga content was 104 ppm on average, while the Tur-I and Tur-II Ga content were 41 ppm on average. At the same time, the study on tourmaline structure also shows that heavy cations Ga can appear at Y and Z site [92]. Cornubian batholith magmatic and early hydrothermal tourmalines have low tin content, with early hydrothermal tourmalines generally containing less than 100 µg/g tin and magmatic tourmalines generally containing less than 20 µg/g tin [11,47,93]. The magmatic tourmaline content in the Jiajika X03 vein is significantly higher than 20 µg/g, possibly due to the fact that the available tin of tin-rich tourmaline may be present in the form of Sn^{4+} through the oxidation of n(II) Cl-complexes or the presence of Sn (IV) Cl-complex during crystallization [94]. In some tourmalines with high titanium content, TiO_2 content can be as high as 4.62 wt.% [95]. Lack of aluminum is a key feature of titanic-rich tourmaline, and the aluminum-rich and titanic-deficient tourmaline in the Jiajika X03 vein also supports this view. Vereshchagin [95] found that at high temperature ($\geq$700 °C), pressure has an adverse effect on the incorporation of titanium in tourmaline structure, on the contrary, at relatively low pressure, the incorporation of titanium in tourmaline structure is controlled by the content of titanium in the mineral forming medium. The main body of pegmatite is formed at 600–150 °C, and the mineralization of rare metals usually occurs between 500–300 °C [80]. The TiO_2 content in the Jiajika X03 vein is low, so the amount of titanium is less in tourmaline structure. Meanwhile, Vereshchagin et al. [96] showed that tourmaline can incorporate large amounts of Pb^{2+}(up to 0.71 apfu) at the X-site. Natural lead-rich tourmalines (such as [97]) thus (1) belong to the Ca-group (based on the dominant-valence rule), and (2) are new members of the tourmaline supergroup (^{X}Pb > 0.5 apfu (Tur-I and Tur-II). Van Hinsberg [98] believed that tourmaline could not separate trace elements significantly. This also means that removal of tourmaline from melt by crystal fractionation does not leave a strong imprint on the map of trace elements except for boron. As a first approximation, this allows the tourmaline component to be used as a direct representation of trace elements in the melt component.

The positive correlation between Mn and Li was closely related to the separation and crystallization of pegmatite/granite [99]. According to London [100], for most Li–Cs-Ta (LCT)-type pegmatite, the residual melt became more Mn rich as the degree of crystallization increased. However, different minerals have different control behaviors on Mn in the melt. For example, the pegmatite melt gradually became Mn poor due to garnet crystallization, while tourmaline crystallization led to Mn enrichment in the residual melt [101]. According to Tindle et al. [99], the relationship between Zn and Li was complex, and their correlation could vary in different pegmatites. By comparing the tourmalines in pegmatite of the East Qinling and Keketohai No. 3 veins, the tourmalines have a high Zn content in the lithium-rich pegmatite. Based on the above analysis, the surrounding rock of the Jiajika X03 vein pegmatite showed strong tourmalinization, indicating potential material exchange between pegmatite and surrounding rock [99]. By comparing the components of tourmaline Tur-I, Tur-II and Tur-IV, the contents of Mg, Ti and V in tourmaline Tur-I and Tur-II were significantly higher than those in the core and mantle of Tur-IV tourmaline, and the edge of Tur-IV tourmaline had higher Ti relative to its core and edge. This indicated that Ti was added to pegmatite in the two-mica quartz schist surrounding rock during Tur-IV tourmaline crystallization. According to Marks et al. [10], the V content of tourmaline in pegmatite surrounding rock (approximately 200×10^{-6}~350×10^{-6}) was significantly higher than that of magmatic tourmaline in pegmatite ($<50 \times 10^{-6}$), which was consistent with the test results from our study (Supplementary Table S1). Therefore, the V content in tourmaline could provide a better indication of whether tourmaline was affected by the addition from the surrounding rock materials. By comparing the tourmaline composition in the Jiajika X03 vein pegmatite, the tourmaline edge of Tur-IV was not affected by the material exchange between the pegmatite and surrounding rock (the V content is basically

unchanged), and the tourmaline core and mantle parts were not significantly reformed. Therefore, the Li, Mn, Zn, Mg and V contents in the schorl tourmaline of the Jiajika X03 vein pegmatite were good indicators of the mineralization type of pegmatite [4]; however, the Ti content in tourmaline was not suitable to indicate the mineralization type of pegmatite due to its interaction between pegmatite and surrounding rock.

In terms of B isotopic composition, the $\delta^{11}B$ value of tourmaline decreases gradually from Tur-I tourmaline to Tur-IV tourmaline. Trumbull et al. [4] showed that crystallization, fluid dissolution and interaction with B-rich surrounding rocks of tourmaline and muscovite could affect the B isotopic composition of the pegmatite system. In addition, Maner and London [12] indicated that the B isotopic composition of the source region determined the $\delta^{11}B$ of tourmaline in pegmatite. Under the condition of the rapid cooling of pegmatite, the growth rate of tourmaline is greater than the diffusion rate of B in pegmatite melt, and magmatic tourmaline $\delta^{11}B$ roughly reflects the $\delta^{11}B$ of the pegmatite melt [12,102,103]. The $\delta^{11}B$ values of Tur-III and Tur-IV tourmalines crystallized from the melt in the Jiajika X03 vein are representative of the $\delta^{11}B$ values of a pegmatite melt. There is a clear correlation between $\delta^{11}B$ and the Li, Zn, Ti and Mn contents in the Jiajika X03 vien tourmaline. Compared with the Tur-II tourmalines, the Tur-IV tourmalines have lower $\delta^{11}B$, higher Li, Mn and Zn contents and lower Ti contents. With the transition of the pegmatite mineralization type from the nonmineralization to Li-rich stage, the $\delta^{11}B$ of tourmaline of the same type decreases, the Li, Mn and Zn contents increase, and the V and Mg contents decrease, which is consistent with the tourmaline composition trend with increasing pegmatite crystallization differentiation [4]. Therefore, the Li, Mn, Zn, Mg and V contents of tourmaline in the Jiajika X03 vein pegmatite are good indicators of the mineralization type of the pegmatite.

6. Conclusions

In our study, the tourmaline in drill hole ZK1101 from the Jiajika X03 vein was divided into four types: two-mica quartz schist (Tur-I), tourmaline hornfels (Tur-II), tourmaline-bearing granite pegmatite (Tur-III) and tourmaline-bearing granite pegmatite (Tur-IV). Through the analyses of major elements, in situ trace elements and boron isotopes, the following conclusions are drawn:

1. Compositionally, these tourmalines belong to the alkali group, and are schorl–Oxy/Fluor–schorl, dravite–Hydroxy-dravite and foitite–Oxy foitite solid solutions. The Tur-I type belong to dravite, the Tur-II type belong to foitite, and the Tur-III and Tur-IV types belong schorl. Petrography, chemical discrimination diagrams and Al occupations at the Y-site indicate that the Tur-III and Tur-IV tourmalines originate from magma and that the Tur-I and Tur-II tourmalines originate from the hydrothermal fluid.

2. Tourmalines from the Jiajika X03 vein have a range of B isotopic compositions from −11.47‰ to −4.93‰, which is typical for S-type granites worldwide. Boron isotopic variations in tourmaline are controlled by fractionation between melt-fluid, tourmaline-fluid and Rayleigh fractionation.

3. The magmatic-hydrothermal transitional stage is critical to Zn enrichment, whereas the high Zn content of the tourmalines can be act as a useful exploration tool to target mineralization.

4. The Li, Mn, Zn, Mg and V contents of tourmaline in nonmineralized pegmatite and lithium mineralized pegmatite in the Jiajika X03 vein is significantly correlated with the B isotope value, indicating that the evolution differentiation of pegmatite is enhanced, and the contents are also good indicators of the type of pegmatite mineralization.

References

1. Jiang, S.Y.; Palmer, M.R. Boron isotope systematics of tourmaline from granites and pegmatites: A synthesis. *Eur. J. Mineral.* **1998**, *10*, 1253–1266. [CrossRef]
2. Hervig, R.L.; Moore, G.M.; Williams, L.B.; Peacock, S.M.; Holloway, J.R.; Roggensack, K. Isotopic and elemental partitioning of boron between hydrous fluid and silicate melt. *Am. Mineral.* **2002**, *87*, 769–774. [CrossRef]
3. Sunde, Ø.; Friis, H.; Andersen, T.; Trumbull, R.B.; Wiedenbeck, M.; Lyckberg, P.; Agostini, S.; Casey, W.H.; Yu, P. Boron isotope composition of coexisting tourmaline and hambergite in alkaline and granitic pegmatites. *Lithos* **2020**, *352–353*, 105293. [CrossRef]
4. Trumbull, R.B.; Beurlen, H.; Wiedenbeck, M.; Soares, D.R. The diversity of B-isotope variations in tourmaline from rare-element pegmatites in the Borborema Province of Brazil. *Chem. Geol.* **2013**, *352*, 47–62. [CrossRef]
5. Siegel, K.; Wagner, T.; Trumbull, R.B.; Jonsson, E.; Matalin, G.; Wälle, M.; Heinrich, C.A. Stable isotope (B, H, O) and mineral-chemistry constraints on the magmatic to hydrothermal evolution of the Varuträsk rare-element pegmatite (northern Sweden). *Chem. Geol.* **2016**, *421*, 1–16. [CrossRef]
6. Feng, Y.G.; Liang, T.; Wang, M.X.; Zhang, Z.; Hao, Y.Y.; Cen, J.B.; Dong, Z.Y. Geochemistry of tourmaline from granitic pegmatites in East Qinling and its implications for mineralization. *Acta Petrol. Sin.* **2022**, *38*, 428–451. (In Chinese with English Abstract)
7. Keller, P.; Robles, E.R.; Pérez, A.P.; Fontan, F. Chemistry, paragenesis and significance of tourmaline in pegmatites of the Southern Tin Belt, central Namibia. *Chem. Geol.* **1999**, *158*, 203–225. [CrossRef]
8. Selway, J.B.; Novák, M.; Cerny, P.; Hawthorne, F.C. Compositional evolution of tourmaline in lepidolite-subtype pegmatites. *Eur. J. Mineral.* **1999**, *11*, 569–584. [CrossRef]
9. Jiang, S.Y.; Radvanec, M.; Nakamura, E.; Palmer, M.; Kobayashi, K.; Zhao, H.X.; Zhao, K.D. Chemical and boron isotopic variations of tourmaline in the Hnilec granite-related hydrothermal system, Slovakia: Constraints on magmatic and metamorphic fluid evolution. *Lithos* **2008**, *106*, 1–11. [CrossRef]
10. Marks, M.A.W.; Marschall, H.R.; Schühle, P.; Guth, A.; Wenzel, T.; Jacob, D.E.; Barth, M.; Markl, G. Trace element systematics of tourmaline in pegmatitic and hydrothermal systems from the Variscan Schwarzwald (Germany): The importance of major element composition, sector zoning, and fluid or melt composition. *Chem. Geol.* **2013**, *344*, 73–90. [CrossRef]
11. Duchoslav, M.; Marks, M.A.W.; Drost, K.; McCammon, C.; Marschall, H.R.; Wenzel, T.; Markl, G. Changes in tourmaline compositionduring magmatic and hydrothermal processes leading to tin-oredeposition: The Cornubian Batholith, SW England. *Ore Geol. Rev.* **2017**, *83*, 215–234. [CrossRef]
12. Maner, J.L.; London, D. The boron isotopic evolution of the Little Three pegmatites, Ramona, CA. *Chem. Geol.* **2017**, *460*, 70–83. [CrossRef]
13. Xiang, L.; Romer, R.L.; Glodny, J.; Trumbull, R.B.; Wang, R.C. Li and B isotopic fractionation at the magmatic-hydrothermal transition of highly evolved granites. *Lithos* **2020**, *376–377*, 105753. [CrossRef]
14. Wang, D.H.; Li, J.K.; Fu, X.F. The metallogenic age of the Jiajika pegmatite type rare metal deposit in Sichuan and its significance. *Geochemistry* **2005**, *34*, 541–547. (In Chinese with English Abstract) [CrossRef]
15. Wang, D.H.; Chen, Y.C. A Preliminary Study on the Composition and Origin of Tourmalines in Dachang, Guangxi. *Acta Petrol. Mineral.* **1996**, *15*, 89–97. (In Chinese with English Abstract)
16. Xu, Z.Q.; Fu, X.F.; Ma, X.X.; Qi, X.X.; Wu, C.; Hou, L.W.; Zhao, Z.B. The gneiss dome and prospecting prospects of the Qinghai-Tibet Plateau. *Acta Geol. Sin.* **2016**, *90*, 2971–2981. (In Chinese with English Abstract)

17. Hou, L.W.; Fu, X.F. *Dome-Like Metamorphic Geological Body on the Eastern Margin of the Songpan-Ganze Orogenic Belt*; Sichuan University Press: Chengdu, China, 2002; pp. 63–111. (In Chinese with English Abstract)

18. Xu, Z.Q.; Liang, B.; Geng, Y.; Liu, T.; Wang, Q.B. Extraction of soils above concealed lithium deposits for rare metal exploration in Jiajika area: A pilot study. *Appl. Geochem.* **2019**, *107*, 142–151. [CrossRef]

19. Liang, B.; Fu, X.F.; Tang, Y. Geochemical characteristics of granites in the Jiajika rare metal mining area in western Sichuan. *J. Guilin Univ. Technol.* **2016**, *36*, 42–49. (In Chinese with English Abstract)

20. Zhang, H.J.; Tian, S.L.; Wang, D.H.; Li, X.F.; Liu, T.; Zhang, Y.J.; Fu, X.F.; Hao, X.F.; Hou, K.J.; Zhao, Y.; et al. Lithium isotope behavior during magmatic differentiation and fluid exsolution in the Jiajika granite–pegmatite deposit, Sichuan, China. *Ore Geol. Rev.* **2021**, *134*, 104139. [CrossRef]

21. Wang, D.H.; Fu, X.F. A breakthrough has been made in the exploration of the Jiajika peripheral lithium deposit in Sichuan. *Rock Miner. Anal.* **2013**, *32*, 987. (In Chinese) [CrossRef]

22. Wang, D.H.; Liu, L.J.; Hou, J.L.; Dai, H.Z.; Yu, Y.; Dai, J.J.; Tian, S.H. A preliminary review of the application of "Five levels + Basement"model for Jiajika-style rare metal deposits. *Earth Sci. Front.* **2017**, *24*, 1–7. (In Chinese with English Abstract) [CrossRef]

23. Wang, D.H.; Liu, S.B.; Yu, Y.; Wang, C.H.; Sun, Y.; Dai, H.Z.; Li, J.K.; Dai, J.J.; Wang, Y.X.; Zhao, D.; et al. Exploration progress and development suggestion for the large-scale mining base of strategic critical mineral resources in western Sichuan. *Acta Geol. Sin.* **2019**, *93*, 1444–1453. (In Chinese with English Abstract) [CrossRef]

24. Fu, X.F.; Liang, B.; Zou, F.G.; Hao, X.F.; Hou, L.W. Discussion on metallogenic geological characteristics and genesisof rare polymetallic ore fields in western Sichuan. *Acta Geol. Sin.* **2021**, *95*, 3054–3068. (In Chinese with English Abstract) [CrossRef]

25. Xu, Z.Q.; Wang, Z.X.; Hou, L.W. New progress in structural studies of Songpan-Ganzi orogenic belt. *Geol. China* **1991**, *15*, 14–16. (In Chinese)

26. Hou, L.W.; Fu, X.F.; Wang, D.H.; Ying, L.J.; Geng, X. Current situation, potential and exploration and developing strategy of rare and dispersed elements mineral resources in Sichuan Province. *Miner. Depos.* **2006**, *25* (Suppl. S1), 523–526. (In Chinese with English Abstract)

27. Liu, S.B.; Yang, Y.Q.; Wang, D.H.; Dai, H.Z.; Ma, S.C.; Liu, L.J.; Wang, C.H. Discovery and significance of granite type lithium industrial orebody in Jiajika orefield, Sichuan Province. *Acta Geol. Sin.* **2019**, *93*, 1309–1320. (In Chinese with English Abstract) [CrossRef]

28. Liu, S.B.; Wang, C.H.; Wang, D.H.; Dai, H.Z.; Ma, S.C.; Yu, Y.; Pan, M.; Hao, X.F.; Yang, R. The "3D2R- BP" large scale mapping method for blocks of pegmatite in the Jiajika deposit, western Sichuan, and significance of its application in the Qinghai-Tibet Plateau. *Acta Geol. Sin.* **2020**, *94*, 326–332. (In Chinese with English Abstract) [CrossRef]

29. Liu, L.J.; Wang, D.H.; Yang, Y.Q.; Fu, X.F.; Hao, X.F.; Pan, M.; Tang, Y.; Chen, Z.Y. Metallogenic characteristics of X03 rare metal vein in Jiajika of Sichuan. *J. Guilin Univ. Technol.* **2016**, *36*, 50–59. (In Chinese with English Abstract)

30. Aysal, N.; Öngen, S.; Hanilçi, N.; Kasapçı, C.; Laçin, D.; Boroğlu, M.Ş.; Yesiltas, M.; Yılmaz, İ.; Azaz, D. Late magmatic— Hydrothermal tourmaline occurrences within leucogranites in NW Anatolia (Turkey): Mineral chemistry and genetic implications. *Geochemistry* **2021**, *81*, 125676. [CrossRef]

31. Liang, B.; Fu, X.F.; Li, S.H.; Tang, Y.; Pan, M.; Hao, X.F. Distribution and occurrence of Cs and other rare elements in contact metamorphic rocks of X03 supergiant deposit in Jiajika, Sichuan and its comprehensive utilization suggestion. *Geol. China* **2022**, *49*, 1214–1223. (In Chinese with English Abstract)

32. Fu, X.F.; Yuan, L.P.; Wang, D.H.; Hou, L.W.; Pan, M.; Hao, X.F.; Liang, B.; Tang, Y. Mineralization characteristics and prospecting model of newly discovered X03 rare metal vein in Jiajika orefield, Sichuan. *Miner. Depos.* **2015**, *34*, 1172–1186. (In Chinese with English Abstract) [CrossRef]

33. Fu, X.F.; Huang, T.; Zou, F.G.; Liang, B.; Hao, X.F.; Yang, R.; Pan, M.; Tang, Y. Ore-controlling mechanism and deep prospecting direction of Jiajika-like lithium mines. *Acta Geol. Sin.* **2021**, *95*, 791–808. (In Chinese with English Abstract) [CrossRef]

34. Hou, K.J.; Li, Y.H.; Xiao, Y.K.; Liu, F.; Tian, Y.R. LA-MC-ICP-MS Technique for in situ measurement of boron isotope microregions. *Chin. Sci. Bull.* **2010**, *55*, 2207–2213. (In Chinese) [CrossRef]

35. Yavuz, F.; Karakaya, N.; Yıldırım, D.K.; Karakaya, M.C.; Kumral, M. A Windows program for calculation and classification of tourmaline-supergroup (IMA-2011). *Comput. Geosci.* **2014**, *63*, 70–87. [CrossRef]

36. Henry, D.J.; Novák, M.; Hawthorne, F.C.; Ertl, A.; Dutrow, B.L.; Uher, P.; Pezzotta, F. Nomenclature of the tourmaline-supergroup minerals. *Am. Mineral.* **2011**, *96*, 895–913. [CrossRef]

37. Hawthorne, F.C.; Henrys, D.J. Classification of the minerals of thetourmaline group. *Eur. J. Mineral.* **1999**, *11*, 201–216. [CrossRef]

38. Henry, D.J.; Guidotti, C.V. Tourmaline as a petrogenetic indicator mineral: An example from the staurolite-grade metapelites of NW Maine. *Am. Miner.* **1985**, *70*, 1–15.

39. Dutrow, B.L.; Henry, D.J. Tourmaline: A geologic DVD. *Elements* **2011**, *7*, 301–306. [CrossRef]

40. Dutrow, B.L.; Henry, D.J. Fibrous tourmaline: A sensitive probe of fluid compositions and petrologic environments. *Can. Miner.* **2016**, *54*, 311–335. [CrossRef]

41. Slack, J.F.; Trumbull, R.B. Tourmaline as a recorder of ore-forming processes. *Elements* **2011**, *7*, 321–326. [CrossRef]

42. Van Hinsberg, V.J.; Henry, D.J.; Dutrow, B.L. Tourmaline as a petrologic forensic mineral: A unique recorder of its geologic past. *Elements* **2011**, *7*, 327–332. [CrossRef]

43. Van Hinsberg, V.J.; Henry, D.J.; Marschall, H.R. Tourmaline: An ideal indicator of its host environment. *Can. Mineral.* **2011**, *49*, 1–16. [CrossRef]

44. London, D.; Manning, D.A. Chemical variation and significance of tourmaline from Southwest England. *Econ. Geol.* **1995**, *90*, 495–519. [CrossRef]

45. London, D.; Morgan, G.B.; Wolf, M.B. Boron in granitic rocks and their contact aureoles. *Rev. Mineral.* **1996**, *33*, 299–330.

46. Li, M.Z.; Qin, Y.L.; Li, Z.; Xu, Y.F.; Wu, W.H.; Liu, W.; Ye, Y.K.; Zhou, X. Geochemical characteristics of two-mica granite and granite pegmatite in Jiajika area, western Sichuan, and their geological implications. *Acta Petrol. Mineral.* **2018**, *37*, 366–378. (In Chinese with English Abstract)

47. Drivenes, K.; Larsen, R.B.; Müller, A.; Sørensen, B.E.; Wiedenbeck, M.; Raanes, M.P. Late-magmatic immiscibility during batholith formation: Assessment of B isotopes and trace elements in tourmaline from the Land's End granite, SW England. *Contrib. Mineral. Petrol.* **2015**, *169*, 56. [CrossRef]

48. Yang, S.Y.; Jiang, S.Y.; Zhao, K.D.; Dai, B.Z.; Yang, T. Tourmaline as a recorder of magmatic-hydrothermal evolution: An in situ major and trace element analysis of tourmaline from the Qitianling batholith, South China. *Contrib. Mineral. Petrol.* **2015**, *170*, 42. [CrossRef]

49. Sokolov, P.B.; Gorskaya, M.G.; Kretser, Y.L. Zinc-bearing tourmalines from raremetal pegmatites. *Zap. Vses. Mineral. Obshchest.* **1988**, *117*, 70–74. (In Russian)

50. Pieczka, A.; Gołebiowska, B.; Jelen, P.; Włodek, A.; Szełeg, E.; Szuszkiewicz, A. Towards Zn-Dominant Tourmaline: A Case of Zn-Rich Fluor-Elbaite and Elbaite from the Julianna System at Piława Górna, Lower Silesia, SW Poland. *Minerals* **2018**, *8*, 126. [CrossRef]

51. Trumbull, R.B.; Garda, G.M.; Xavier, R.P.; Cavalcanti, J.A.D.; Codeço, M.S. Tourmaline in the Passagem de Mariana gold deposit (Brazil) revisited: Major-element, trace-element and B-isotope constraints on metallogenesis. *Miner. Depos.* **2018**, *54*, 395–414. [CrossRef]

52. Qiao, X.Y.; Li, W.B.; Zhang, L.J.; White, N.C.; Zhang, F.H.; Yao, Z.W. Chemical and boron isotope compositions of tourmaline in the Hadamiao porphyry gold deposit, Inner Mongolia, China. *Chem. Geol.* **2019**, *519*, 39–55. [CrossRef]

53. Bea, F.; Pereira, M.D.; Stroh, A. Mineral/leucosome trace element partitioning in a peraluminous migmatite (a laser ablation-ICP-MS study). *Chem. Geol.* **1994**, *117*, 291–312. [CrossRef]

54. Nash, W.P.; Crecraft, H.R. Partition coefficients for trace elements in silicic magmas. *Geochem. Cosmochim. Acta* **1985**, *49*, 2309–2322. [CrossRef]

55. Kogiso, T.; Tatsumi, Y.; Nakano, S. Trace element transport during dehydration processes in the subducted oceanic crust: Experiments implications for the origin of ocean island basalts. *Earth Planet. Sci. Lett.* **1997**, *148*, 193–205. [CrossRef]

56. Shore, M.; Fowler, A.D. Oscillatory zoning in minerals; a common phenomenon. *Can. Mineral.* **1996**, *34*, 1111–1126.

57. Holten, T.; Jamtveit, B.; Meakin, P.; Cortini, M.; Blundy, J.; Austrheim, H. Statistical characteristics and origin of oscillatory zoning in crystals. *Am. Mineral.* **1997**, *82*, 596–606. [CrossRef]

58. Launay, G.; Sizaret, S.; Lach, P.; Melleton, J.; Gloaguen, E.; Poujol, M. Genetic relationship between greisenization and Sn-W mineralizations in vein and greisen deposits: Insights from the Panasqueira deposit (Portugal). *BSGF Earth. Sci. Bull.* **2021**, *192*, 2. [CrossRef]

59. Marschall, H.R.; Ludwig, T.; Altherr, R.; Kalt, A.; Tonarini, S. Syros metasomatic tourmaline: Evidence for very high-delta B11 fluids in subduction zones. *J. Petrol.* **2006**, *47*, 1915–1942. [CrossRef]

60. Trumbull, R.B.; Codeço, M.S.; Jiang, S.Y.; Palmer, M.R.; Slack, J.F. Boron isotope variations in tourmaline from hydrothermal ore deposits: A review of controlling factors and insights for mineralizing systems. *Ore Geol. Rev.* **2020**, *125*, 103682. [CrossRef]

61. Marschall, H.R.; Jiang, S.Y. Tourmaline isotopes: No element left behind. *Elements* **2011**, *7*, 313–319. [CrossRef]

62. Palmer, M.R.; Slack, J.F. Boron isotopic composition of tourmaline from massive sulfide deposits and tourmalinites. *Contrib. Mineral. Petrol.* **1989**, *103*, 434–451. [CrossRef]

63. Su, Z.K.; Zhao, X.F.; Li, X.C.; Zhou, M.F. Using elemental and boron isotopic compositions of tourmaline to trace fluid evolutions of IOCG systems: The world-class Dahongshan Fe-Cu deposit in SW China. *Chem. Geol.* **2016**, *441*, 265–279. [CrossRef]

64. Zhao, Z.; Xya, B.; Qla, B.; Ylab, C.; Sca, B.; Chao, S.; Wab, H.; Shuang, L.D. In-situ boron isotopic and geochemical compositions of tourmaline from the Shangbao Nb-Ta bearing monzogranite, Nanling Range: Implication for magmatic-hydrothermal evolution of Nb and Ta. *Lithos* **2021**, *386–387*, 106010. [CrossRef]

65. Codeco, M.S.; Weis, P.; Trumbull, R.B.; Pinto, F.; Lecumberri-Sanchez, P.; Wilke, F.D.H. Chemical and boron isotopic composition of hydrothermal tourmaline from the Panasqueira W-Sn-Cu deposit, Portugal. *Chem. Geol.* **2017**, *468*, 1–16. [CrossRef]

66. Meyer, C.; Wunder, B.; Meixner, A.; Romer, R.L.; Heinrich, W. Boron-isotope fractionation between tourmaline and fluid: An experimental re-investigation. *Contrib. Mineral. Petrol.* **2008**, *156*, 259–267. [CrossRef]

67. Palmer, M.; London, D.; Morgan, G.B., VI; Babb, H. Experimental determination of fractionation of $^{11}B/^{10}B$ between tourmaline and aqueous vapor: A temperature-and pressure-dependent isotopic system. *Chem. Geol.* **1992**, *101*, 123–129. [CrossRef]

68. Kasemann, S.; Erzinger, J.; Franz, G. Boron recycling in the continental crust of the Central Andes from the Palaeozoic to Mesozoic, NW Argentina. *Contrib. Mineral. Petrol.* **2000**, *140*, 328–343. [CrossRef]

69. Chaussidon, M.; Albarède, F. Secular boron isotope variations in the continental crust: An ion microprobe study. *Earth Planet. Sci. Lett.* **1992**, *108*, 229–241. [CrossRef]

70. Xavier, R.P.; Wiedenbeck, M.; Trumbull, R.B.; Dreher, A.M.; Monteiro, L.V.S.; Rhede, D.; de Araújo, C.E.G.; Torresi, I. B-isotopes fingerprint marine evaporites as the source of high-salinity ore fluids in iron oxide copper-gold deposits. *Carajás Miner. Prov. Geol.* **2008**, *36*, 743–746.

71. Hou, J.L. The Comparative Study of Diagenetic, Metallogenic Characteristics and Tectonic Environment of Two Kinds of Pegmatites in China. Ph.D. Thesis, Chinese Academy of Geological Sciences, Beijing, China, 2018.

72. Barton, M.D. Iron oxide (Cu-Au-REE-P-Ag-U-Co) systems. In *Geochemistry of Mineral Deposits*; Treatise on Geochemistry; Scott, S.D., Ed.; Elsevier: Amsterdam, The Netherlands, 2014; pp. 515–541.

73. Smith, M.P.; Yardley, B.W.D. The boron isotopic composition of tourmaline as a guide to fluid processes in the southwestern England orefield: An ion microprobe study. *Geochim. Cosmochim. Acta* **1996**, *60*, 1415–1427. [CrossRef]

74. Zhang, S.T.; Ma, D.S.; Lu, J.J.; Zhang, R.Q.; Gao, S.Y. Chemical and boron isotopic composition of tourmaline in Baotan tin deposit, northern Guangxi, South China. *Acta Geol. Sin.* **2014**, *88*, 485–486. [CrossRef]

75. Kaliwoda, M.; Marschall, H.R.; Marks, M.A.; Ludwig, T.; Altherr, R.; Markl, G. Boron and boron isotope systematics in the peralkaline Ilímaussaq intrusion (South Greenland) and its granitic country rocks: A record of magmatic and hydrothermal processes. *Lithos* **2011**, *125*, 51–64. [CrossRef]

76. Kowalski, P.M.; Wunder, B.; Jahn, S. Ab initio prediction of equilibrium boron isotope fractionation between minerals and aqueous fluids at high P and T. *Geochim. Cosmochim. Acta* **2013**, *101*, 285–301. [CrossRef]

77. Guo, J.; Lu, X.A.; Rzb, C.; Tao, Y.B.; Kai, W.D.; Ws, E. Chemical and boron isotopic variations of tourmaline deciphering magmatic-hydrothermal evolution at the Gejiu Sn-polymetallic district, South China. *Chem. Geol.* **2022**, *593*, 120698. [CrossRef]

78. Marschall, H.R.; Foster, G. (Eds.) Boron isotopes in the ocean floor realm and the mantle. In *Advances in Isotope Geochemistry-Boron Isotopes—The Fifth Element*; Springer: Berlin/Heidelberg, Germany, 2018; pp. 189–215.

79. Li, Y.; Zou, H.; Said, N.; Liu, H. A new classification of barite deposits in China. *Ore Energy Resour. Geol.* **2023**, *14*, 100019. [CrossRef]

80. Cao, H.W.; Pei, Q.M.; Yu, X.; Cao, A.B.; Chen, Y.; Liu, H.; Zhang, K.; Liu, X.; Zhang, X.F. The long–lived partial melting of the Greater Himalayas in southern Tibet, constraints from the Miocene Gyirong anatectic pegmatite and its prospecting potential for rare element minerals. *China Geol.* **2023**, *6*, 303–321.

81. Zhang, W.; Qin, S.; Zhang, W.L.; Liu, H.; Zhang, K.; Liu, X.; Zhang, X.F.; Cao, H.W. A timeline of the Cenozoic tectonic–magmatic–metamorphic evolution and development of ore resources in the Himalayas. *Geol. J.* **2023**, 1–18. [CrossRef]

82. Telus, M.; Dauphas, N.; Moynier, F.; Tissot, F.L.H.; Teng, F.Z.; Nabelek, P.L.; Craddock, P.R.; Grpat, L.A. Iron, zinc, magnesium and uranium isotopic fractionation during continental crust differentiation: The tale from migmatites, granitoids, and pegmatites. *Geochim. Cosmochim. Acta* **2012**, *97*, 247–265. [CrossRef]

83. Richards, J.P.; Kerrich, R.W. Special paper: Adakite-like rocks: Their diverse origins and questionable role in metallogenesis. *Econ. Geol.* **2007**, *102*, 537–576. [CrossRef]

84. Chiaradia, M.; Ulianov, A.; Kouzmanov, K.; Beate, B. Why large porphyry Cu deposits like high Sr/Y magmas? *Sci. Rep.* **2012**, *2*, 685. [CrossRef]

85. Loucks, R.R. Distinctive composition of copper-oreforming arcmagmas. *Aust. J. Earth Sci.* **2014**, *61*, 5–16. [CrossRef]

86. Aigner-Torres, M.; Blundy, J.; Ulmer, P.; Pettke, T. Laser ablation ICP-MS study of trace element partitioning between plagioclase and basaltic melts: An experimental approach. *Contrib. Mineral. Petrol.* **2007**, *153*, 647–667. [CrossRef]

87. Li, Y.; Audetat, A.; Liu, Z.; Wang, F. Chalcophile element partitioning between Cu-rich sulfide phases and silicate melt and implications for the formation of Earth's continental crust. *Geochim. Cosmochim. Acta* **2021**, *302*, 61–82. [CrossRef]

88. Rudnick, R.L.; Gao, S. Composition of the continental crust. *Treatise Geochem.* **2003**, *3*, 1–64.

89. Prokofev, V.Y.; Naumov, V.B.; Dorofeeva, V.A. Gallium concentration in natural melts and fluids. *Geochem. Int.* **2016**, *54*, 691–705. [CrossRef]

90. Breiter, K.; Gardenova, N.; Kanicky, V.; Vaculovic, T. Gallium and germanium geochemistry during magmatic fractionation and post-magmatic alteration in different types of granitoids: A case study from the Bohemian Massif (Czech Republic). *Geol. Carpathica* **2013**, *64*, 171–180. [CrossRef]

91. Sciuba, M.; Beaudoin, G.; Makvandi, S. Chemical composition of tourmaline in orogenic gold deposits. *Miner. Depos.* **2021**, *56*, 537–560. [CrossRef]

92. Vereshchagin, O.S.; Setkova, T.V.; Rozhdestvenskaya, I.V.; Frank-Kamenetskaya, O.V.; Deyneko, D.V.; Pokholok, K.V. Synthesis and crystal structure of Ga-rich, Fe-bearing tourmaline. *Eur. J. Mineral.* **2016**, *28*, 593–599. [CrossRef]

93. Drivenes, K.; Brownscombe, W.; Larsen, R.B.; Seltmann, R.; Spratt, J.; Sørensen, B.E. Classification and characterisation of magmatic–hydrothermal tourmaline by combining field observations and microanalytical techniques. *IOP Conf. Ser. Mater Sci. Eng.* **2020**, *891*, 012010. [CrossRef]

94. Drivenes, K. Sn-rich tourmaline from the Land's End granite, SW England. *J. Geosci.* **2022**, *67*, 173–189. [CrossRef]

95. Vezzoni, S.; Biagioni, C.; D'Orazio, M.; Pieruccioni, D.; Galanti, Y.; Petrelli, M.; Molli, G. Evidence of Permian magmatism in the Alpi Apuane metamorphic complex (Northern Apennines, Italy): New hints for the geological evolution of the basement of the Adria plate. *Lithos* **2018**, *318–319*, 104–123. [CrossRef]

96. Vereshchagin, O.S.; Wunder, B.; Britvin, S.N.; Frank-Kamenetskaya, O.V.; Wilke, F.D.H.; Vlasenko, N.S.; Shilovskikh, V.V. Synthesis and crystal structure of Pb-dominant tourmaline. *Am. Mineral.* **2020**, *105*, 1589–1592.

97. Sokolov, M.; Martin, R.F. A Pb-dominant member of the tourmaline group, Minh Tien granitic pegmatite, Luc Yen district, Vietnam. *Estud. Geológicos* **2009**, *19*, 352–353.

98. Van Hinsberg, V.J. Preliminary experimental data on trace-element partitioning between tourmaline and silicate melt. *Can. Mineral.* **2011**, *49*, 153–163. [CrossRef]

99. Tindle, A.G.; Breaks, F.W.; Selway, J.B. Tourmaline in petalite-subtype granitic pegmatites: Evidence of fractionation and contamination from the Pakeagama Lake and Separation Lake areas of northwestern Ontario, Canada. *Can. Mineral.* **2002**, *40*, 753–788. [CrossRef]
100. London, D. Pegmatites. The Canadian Mineralogist. *Spec. Publ.* **2008**, *10*, 1–347.
101. Maner, J.L.; London, D.; Icenhower, J.P. Enrichment of manganese to spessartine saturation in granite-pegmatite systems. *Am. Mineral.* **2019**, *104*, 1625–1637. [CrossRef]
102. Li, J.K.; Fu, X.F.; Zou, T.R.; Wang, D.H. Prospecting breakthrough and outlying prospecting prospect analysis of the lithium Jiajika deposit in Sichuan Province. *Miner. Depos.* **2014**, *33* (Suppl. S1), 1175–1176. (In Chinese)
103. Liu, L.J.; Wang, D.H.; Dai, H.Z.; Hou, J.L. Geochemical Characteristics of REE and Its Implications to X03 Super-Large Lithium Pegmatite Vein, Jiajika, Sichuan. *Earth Sci.* **2017**, *42*, 1673–1683. (In Chinese with English Abstract)